Single cell transcriptome analysis of cavernous tissues reveals the key roles of pericytes in diabetic erectile dysfunction

Seo-Gyeong Bae[1†], Guo Nan Yin[2†], Jiyeon Ock[2†], Jun-Kyu Suh[2*], Ji-Kan Ryu[2,3*], Jihwan Park[1*]

[1]School of Life Sciences, Gwangju Institute of Science and Technology (GIST), Gwangju, Korea

[2]National Research Center for Sexual Medicine and Department of Urology, Inha University School of Medicine, Incheon, Korea

[3]Program in Biomedical Science & Engineering, Inha University, Incheon, Korea

†These authors contributed equally to this work.

*Corresponding authors

Jun-Kyu Suh, MD, PhD

National Research Center for Sexual Medicine and Department of Urology, Inha University School of Medicine

100 Inha-ro, Michuhol-gu, Incheon, Republic of Korea, 22212

E-mail: jksuh@inha.ac.kr

Ji-Kan Ryu, MD, PhD

National Research Center for Sexual Medicine and Department of Urology, Inha University School of Medicine

100 Inha-ro, Michuhol-gu, Incheon, Republic of Korea, 22212

E-mail: rjk0929@inha.ac.kr

Jihwan Park, PhD

School of Life Sciences, Gwangju Institute of Science and Technology

123 Cheomdangwagi-ro, Buk-gu, Gwangju, Republic of Korea, 61005

Tel: +82-62-715-2503 Fax: +82-62-715-2484 E-mail: jihwan.park@gist.ac.kr

Abstract

Erectile dysfunction (ED) affects a significant proportion of men aged 40–70 and is caused by cavernous tissue dysfunction. Presently, the most common treatment for ED is phosphodiesterase 5 inhibitors; however, this is less effective in patients with severe vascular disease such as diabetic ED. Therefore, there is a need for development of new treatment, which requires a better understanding of the cavernous microenvironment and cell-cell communications under diabetic condition. Pericytes are vital in penile erection; however, their dysfunction due to diabetes remains unclear. In this study, we performed single-cell RNA sequencing to understand the cellular landscape of cavernous tissues and cell type-specific transcriptional changes in diabetic ED. We found a decreased expression of genes associated with collagen or extracellular matrix organization and angiogenesis in diabetic fibroblasts, chondrocytes, myofibroblasts, valve-related lymphatic endothelial cells, and pericytes. Moreover, the newly identified pericyte-specific marker, LBH, in mouse and human cavernous tissues, clearly distinguishing pericytes from smooth muscle cells. Cell–cell interaction analysis revealed that pericytes are involved in angiogenesis, adhesion, and migration by communicating with other cell types in the corpus cavernosum; however, these interactions were highly reduced under diabetic conditions. LBH expression is low in diabetic pericytes, and overexpression of LBH prevents erectile function by regulating neurovascular regeneration. Furthermore, the LBH-interacting proteins (CRYAB and VIM) were identified in mouse cavernous pericytes through LC-MS/MS analysis, indicating that their interactions were critical for maintaining pericyte function. Thus, our study reveals novel targets and insights into the pathogenesis of ED in patients with diabetes.

Keywords

diabetes; erectile dysfunction; pericyte; single-cell RNA sequencing

Introduction

Erectile dysfunction (ED) is an age-dependent vascular disease, affecting 5–35% of men aged 40–70 in varying degrees [1]. Although not fatal, 322 million men worldwide will be affected by the disease by 2025 [2,3]. Moreover, it occurs in up to 75% of diabetes cases, especially in men [4]. This causes significant physical and psychological problems for patients and their families [5]. Moreover, the cavernous tissue is more prone to this disease than other blood vessels; therefore, its malfunction is considered as a biomarker in the progression of cardiovascular and vascular diseases [6]. Current ED treatment involves the use of phosphodiesterase 5 (PDE5) inhibitors, but patients with severe vascular disease, such as diabetic ED, are less responsive. This is mainly because severe vascular dysfunction caused by diabetes results in insufficient bioavailable NO for PDE5 inhibitors to induce penile erection [7]. Therefore, it is necessary to identify novel therapeutic targets, which requires a comprehensive understanding of the cavernous microenvironment, including cell–cell interactions, regulatory signals, and molecular regulation. Although recent studies have proposed gene expression profiles of primary cultured cavernous cells exposed to hyperglycemic conditions [8-10], the relevant cell-specific relationships and genetic mechanisms in cavernous tissues have not been elucidated yet.

Pericytes are vital in the pathogenesis of erectile function as their interactions with ECs are essential for penile erection. Pericytes interact with various cell types (especially endothelial cells) and are involved in angiogenesis, vasoconstriction, and permeability [11]. Diabetes causes pericyte loss or dysfunction, thereby creating an imbalance between pericytes and endothelial cells, leading to vascular diseases [12,13]. For example, diabetic retinopathy is characterized by pericyte loss, capillary basement membrane thickening, and increased permeability, leading to retinal hypoxia and inflammation. Pericytes are particularly sensitive to glucose oxidation, which further promotes pericyte apoptosis [13]. Advanced glycation end products (AGEs) accumulate in pericytes under hyperglycemic conditions, thereby stimulating the secretion of TGF□ in peripheral nerve pericytes, leading to basement membrane thickening, neovascularization, and pericyte apoptosis [14]. Furthermore, our previous studies showed that restoring the content and function of cavernous pericytes significantly reduced the permeability of cavernous blood vessels and enhanced neurovascular regeneration [10,15,16]. However, the mechanisms underlying the effect of diabetes on pericyte dysfunction in the ED remain unclear.

Smooth muscle cells are also a vital component of the cavernous tissues in penile erection. Diabetes mellitus leads to smooth muscle cell dysfunction, such as decreased cavernosal smooth muscle relaxation, resulting in an inability to obtain or maintain satisfactory erection [17,18]. Since the marker genes of pericytes and smooth muscle

cells often overlap, and their expression patterns are tissue-specific, identifying suitable *in vivo* markers to accurately interpret transcriptional and phenotypic changes in these cell types is of utmost importance [19-21]. Recent studies have identified pericyte-specific markers in different tissues using single-cell RNA sequencing [22,23], enabling characterization of various cell types and their cell–cell communication. In this study, a single-cell transcriptome analysis was performed to examine the cellular heterogeneity in erectile dysfunction caused by diabetes. The goal of this study was to identify markers specific to cavernous pericytes and understand their role in ED by exploring their interactions with other cell types.

Results

Single cell transcriptional landscape of mouse cavernous tissue

To elucidate the cellular landscape of mouse cavernous tissue and transcriptional changes in diabetic ED at the cellular level, we conducted a single-cell transcriptome analysis, profiling 12,894 cells **(Fig. 1A)**. The cells were grouped into 15 clusters based on their transcriptomic patterns, and cell types were annotated based on the expression of marker genes **(Fig. 1B, C)**. Clustering analysis identified fibroblasts (FB), chondrocytes (Chond), myofibroblasts (Myo-FB), lymphatic endothelial cells (LEC), valve-related LEC, vascular endothelial cells (VEC), smooth muscle cells (SMC), pericytes, Schwann cells, and macrophages. The Chond and FB subsets were further annotated with additional marker genes **(Fig. 1D, E, and Supplementary Fig. 1).**

Furthermore, we analyzed cell type-specific transcriptional changes due to diabetes **(Fig. 1F and Supplementary Fig. 2A-G)**. We found that *Nos3* (highly expressed in the untreated diabetes group compared to the treatment group) decreased in diabetic valve-related LEC and VEC [24]. In addition, *Igfbp2* and *Igfbp4* (lowly expressed in the penis of diabetic rats) were also downregulated in diabetic SMC and chondrocytes, respectively [25], whereas *Igfbp3* was upregulated in diabetic FB and Myo-FB [25]. Collagen genes (vital in the corpus cavernosum structure) were significantly under expressed in diabetic FB, Chond, My-FB, and pericytes than in normal tissues [26]. Gene ontology analysis using differentially expressed genes (DEGs) indicated that the genes associated with collagen or extracellular matrix organization and angiogenesis were downregulated in diabetic FB, Chonds, Myo-FBs, valve-related LEC, and pericytes compared to the cells under normal conditions **(Fig. 1G and Supplementary Fig. 3)**. In contrast, diabetic mice showed an increase in ribosome- and translation-related terms **(Fig. 1H and Supplementary Fig. 4)**. Schwann cells showed an increased expression compared to normal cells in diabetes, though not significant.

Identifying specific markers for pericytes in mouse cavernosum tissues

We distinguished SMC from pericytes by examining the expression of previously known marker genes (*Cnn1* for SMC, *Rgs5* and *Pdgfrb* for pericytes) **(Fig. 2A)**. However, rather than being exclusively expressed in each cell type, known marker genes were co-expressed in each cell type. To ensure proper annotation of SMC and

pericytes, we identified the gene sets enriched in each cluster through gene set enrichment analysis (GSEA). We found that the gene sets matching pericyte and SMC functions were enriched in each cluster **(Fig. 2B)** Gene sets related to the regulation of blood vessels and leukocytes were enriched in pericytes, whereas gene sets related to actin or muscles were enriched in SMC, suggesting that these clusters were properly annotated. In addition, we screened six genes (*Lbh, Ednra, Gpc3, Npy1r, Pln,* and *Atp1b2*) that were specifically expressed in the pericyte cluster from the single-cell analysis results **(Supplementary Fig. 5A)**. The literature search excluded four genes, *Ednra, Gpc3, Npy1r,* and *Pln,* as they are also expressed in the SMCs of other tissues or different cell types [27-30]. *Atp1b2* was also excluded because its protein expression was detected in both mouse cavernous pericytes and aortic SMC using immunofluorescence (IF) staining **(Supplementary Fig. 5B)**. In the single-cell data, *Lbh* (Limb Bud-Heart) was more specific for pericytes than *Rgs5*, a well-known marker for distinguishing between SMC and pericytes **(Fig. 2A, C)**. From our IF staining, we found that LBH was optimally expressed in mouse cavernous pericyte, whereas it was rarely expressed in the smooth muscle cell (SMC) of the aorta, consistent with our single-cell data **(Fig. 2D, top panel)**. We also verified the expression of LBH in blood vessels of other organs such as the bladder, aorta, and kidney by double staining with an endothelial cell marker (CD31) and LBH. In the blood vessels of these organs, CD31-expressing endothelial cells were surrounded by LBH-expressing pericytes but did not merge **(Fig. 2D, bottom panel)**. Finally, we validated whether LBH is a more specific marker of pericyte in different tissues. We found that LBH expression was easily distinguishable from α-SMA in mouse cavernosum, dorsal artery and dorsal vein tissues, and is more specific than traditional pericyte markers (PDGFRβ) through LBH/α-SMA or LBH/PDGFRβ double staining, separately (**Fig. 2E**). For instance, PDGFRβ is expressed in pericytes and other surrounding tissue cells (as indicated by arrows and dotted area). This reveals that LBH is a prospective marker that can easily differentiate pericytes from smooth muscle cells or other mural cells.

Interactions between pericyte and other cell types in diabetes versus normal

Pericytes regulate various physiological functions involving other cell types such as EC and SMC. We compared the cell–cell interactions between pericytes and other cell types based on ligand-receptor interactions in single-cell data from mouse cavernous tissues under normal and hyperglycemic conditions. In diabetes, angiogenesis-related interactions, including vascular endothelial growth factor (VEGF) and fibroblast growth

factor (FGF), were reduced between pericytes and other cell types compared to those under normal conditions **(Fig. 3A-C)**. In addition, interactions related to neuronal survival, adhesion, migration, and proliferation decreased in diabetic mice, as opposed to an increase in BMP signaling-related interactions **(Supplementary Fig. 6 and Supplementary Fig. 7)**. In addition to cell–cell interactions, the overall gene sets associated with angiogenesis, adhesion, and cell migration in pericytes were downregulated under diabetic conditions **(Fig. 3D)**. We performed gene regulatory network analysis to compare the activities of transcription factors (TFs) in pericytes under diabetic and normal conditions. In normal pericytes, TFs promoting angiogenesis (*Klf5*, *Egr1*, *Lmo2*, *Junb*, and *Elk1*) were more active than in diabetic pericytes **(Fig. 3E)**. In contrast, TFs that inhibit angiogenesis (*Ppard* and *Hoxd10*) were more active in diabetes. Furthermore, using the proteome profiler mouse angiogenesis array, we tested 53 angiogenesis factors in cavernous tissue, among which the expression of OPN [31], CD105 [32], IGFBP2 [33], IGFBP9 [34] and TSP-2 [35] decreased under diabetic conditions, and only MMP-3 increased **(Fig. 3F)**. MMP-3 expression in the neurovascular unit is enhanced under diabetic conditions, leading to vascular damage [36]. Thus, angiogenesis activity decreased in mouse cavernous pericytes (MCPs) under diabetic conditions.

LBH improves erectile function under diabetic conditions through enhanced neurovascular regeneration

LBH is vital in promoting angiogenesis in human glioma under hypoxic conditions [37]. We performed IF staining for LBH and another pericyte marker (CD140b) in mouse cavernous tissues to explore the effect of LBH on erectile dysfunction. We found that LBH and CD140b expression significantly decreased in the pericytes under diabetic conditions compared to those in age-matched controls (**Fig. 4A, C**). In addition, we assessed the expression of LBH *in vitro* under diabetic conditions and found that its expression was significantly decreased compared to that under normal conditions in mouse cavernous pericytes (**Fig. 4B, D**). All IF staining results were confirmed by western blotting (**Fig. 4E, F**). In addition, we overexpressed LBH in diabetic mice by intracavernosal injection of lentiviruses containing an ORF mouse clone of LBH and assessed erectile function two weeks later. During electrical stimulation, the ratios of maximal and total intracavernous pressure (ICP) to mean systolic blood pressure (MSBP) were significantly reduced in PBS- and lentivirus ORF control particle-treated diabetic mice compared to age-matched controls. However, LBH overexpression in diabetic mice significantly improved this erection parameter, reaching 84% of the control values (**Fig. 4G, H**). Moreover,

IF staining for CD31 (an endothelial cell marker), NG2 (a pericyte marker), neurofilament-2000 (NF), and neuronal NOS (nNOS) revealed that LBH overexpression significantly improved the endothelial cell, pericyte, and neuronal cell contents in diabetic mice (**Fig. 4I-N**). These effects were achieved by inducing MCPs survival (decreased apoptosis, increased proliferation, migration, and tube formation) and major pelvic ganglion (MPG) neurite sprouting under diabetic conditions (**Supplementary Fig. 8**). Thus, LBH is vital in promoting neurovascular regeneration under diabetic conditions.

Expression of LBH in human cavernous pericytes and its role in diabetic conditions

Using a previous single-cell transcriptomics data of the human corpus cavernosum [38], we examined whether LBH is specifically expressed in human cavernous pericytes and has a similar role in diabetic conditions **(Fig. 5A)**. Further clustering of an SMC cluster (marker: *ACTA2*) in the previous study identified three subclusters; ACTA2-expressing cluster as myofibroblasts (MFBs), *CNN1*-expressing cluster as SMCs, and *RGS5*- and *LBH*-expressing clusters as pericytes **(Fig. 5B)**. Gene Ontology analysis using DEGs between these clusters identified terms related to pericyte function in *LBH*-expressing pericytes (angiogenesis and leukocyte migration) **(Fig. 5C)**. The newly identified pericyte marker, LBH is also a marker of pericytes in the human corpus cavernosum, and LBH expression was significantly reduced in human cavernous tissues from patients with diabetes-induced ED compared to age-matched controls (**Fig. 5D, F**). Furthermore, LBH expression was significantly reduced in primary cultured human cavernous pericytes under diabetic conditions compared to normal glucose conditions (**Fig. 5E, G**).

LBH-interacting protein identification in mouse cavernous pericytes

We conducted LC-MS/MS analysis following the immunoprecipitation of LBH from mouse cavernous pericytes to further elucidate the LBH-mediated systematic network in mouse cavernous pericytes. In protein–protein interaction (PPI) databases, only CRYAB was experimentally confirmed to interact with LBH [39]. However, only the co-fractionation of LBH and CRYAB has been outlined, and direct binding between the two proteins has not been elucidated yet. We identified αB-crystallin (CRYAB) from band 1 and Vimentin (VIM) from band 2, co-immunoprecipitated with LBH (**Fig. 6A, B**). Furthermore, double IF staining indicated that LBH co-localized with CRYAB and VIM in mouse cavernous tissues and MCPs (**Fig. 6C, D**). Thus, CRYAB and VIM are novel LBH-interacting proteins in mouse cavernous pericytes.

Based on the STRING and BioGrid databases, we reconstructed the PPI network of CRYAB, VIM, and LBH, and the primary and secondary interacting proteins of LBH **(Fig. 6E)**. To identify the molecular mechanisms underlying interactions of LBH CRYAB, and VIM, we performed gene ontology analysis using proteins from the PPI network. We found that these proteins are mainly involved in neurogenesis, neuronal development, and the nervous system **(Fig. 6F)**. In addition, the proteins involved in 'angiogenesis' and 'response to estradiol' that are associated with pericyte activity were also included in this PPI network. Since the expression of LBH was decreased in the pericytes under diabetic conditions, we identified the expression level of angiogenesis and nerve system-related genes in diabetic pericytes using single-cell data. GSEA showed that gene sets related to angiogenesis and the nervous system were enriched in normal pericytes compared to diabetic pericytes **(Fig. 6G)**. Finally, we found that CRYAB expression significantly reduced *in vitro* and *in vivo* under diabetic conditions, whereas VIM expression significantly increased (**Fig. 6H, I**). This reveals that the expression of nervous system- and angiogenesis-related genes are downregulated as LBH decreases in pericytes under diabetic conditions, affecting the interacting molecules.

Discussion

DM is a major cause of ED, and poor long-term glycemic control can lead to nerve and blood vessel damage [40]. Many studies have outlined angiogenic and neurotrophic factors, such as VEGF, Comp-Ang1, dickkopf2, leucine-rich alpha-2 glycoprotein 1 (LRG1), brain-derived neurotrophic factor (BDNF), and neurotrophin-3 (NT3) that been tested as therapeutic options for ED [41-46]. However, poor efficacy, side effects such as inflammation, and complex drug-protein engineering have limited their success in clinical trials. A more detailed understanding of the intercellular signaling mechanisms and microenvironment in the penis under physiological and pathological conditions are necessary to provide more effective therapeutic targets. We therefore employed single-cell RNA sequencing to dissect the complex transcriptional changes in various cell types in ED using a diabetes-induced ED mouse model, as diabetic ED accounts for 75% of ED patients [4]. Our findings from *in vivo* animal models and *in vitro* experiments were confirmed using human data and samples, enabling us to understand how the results from mouse models could be translated to humans and developed as novel treatment targets.

To repair vascular and neural tissues in the penile corpus cavernosum damaged by DM, we focused on pericytes, which are multipotent perivascular cells that contribute to the generation and repair of various tissues in response to injury [47]. Although recent studies have shown that pericytes are involved in physiological mechanisms of erection, little is known about their detailed mechanisms. Many known pericyte markers are co-expressed in other cell types; thus, identifying the specific marker genes for pericytes *in vivo* is the first step characterizing pericyte cell type. From the pericyte cluster in the single-cell RNA sequencing results, we found that *Lbh, Ednra, Gpc3, Npy1r, Plm,* and *Atp1b2* are specific pericyte markers (**Supplementary Fig. 6**). LBH was identified as a pericyte-positive and SMC-negative marker that was also specifically expressed in human cavernous pericytes (**Fig. 5**) and was validated through IF staining in many vascular tissues and cell types (**Fig. 2**).

LBH, a highly conserved transcription cofactor, is known to participate in early limb and heart development [48]. Moreover, LBH can directly target the Wnt signaling pathway [49] and regulate neural crest cell development [50]. In addition, Jiang et al. showed that LBH overexpression promotes angiogenesis via VEGF-mediated ERK signaling [37]. In contrast, LBH inhibits cell migration and angiogenesis in nasopharyngeal carcinoma [51,52]. These inconsistent results may be related to different histopathological environments. Thus, LBH has dual effects on

the development of blood vessels and the nervous system, similar to other angioneurins such as VEGF and BDNF [53]. Here, we explored the role of LBH in the penile tissues of diabetic mice. Interestingly, LBH expression was significantly lower in cavernous pericytes in a diabetic mouse model. Therefore, we hypothesized that the restoration of LBH expression in the penis of diabetic mice will improve erectile function. Our results showed that LBH can restores diabetes-induced ED by restoring neurovascular regeneration (**Fig. 3**).

Previous studies have shown that CRYAB promotes angiogenesis [54] and interacts with LBH in nasopharyngeal carcinoma cells, where it enhances cell survival by inhibiting the autoproteolytic maturation of caspase-3 [52]. Interestingly, our LC-MS/MS analysis of LBH following immunoprecipitation of MCPs identified VIM as a novel interaction partner and CRYAB (**Fig. 5**). In addition, we assessed the expression of CRYAB and VIM under diabetic conditions. Unexpectedly, the expression of VIM was increased, whereas that of CRYAB was downregulated in the penis of diabetic mice and MCPs under diabetic conditions. VIM is a type III intermediate filament protein expressed in mesenchymal cells [55,56]. It is involved in cell adhesion, migration, cellular integrity, epithelial-mesenchymal transition, and the malignant transformation and metastatic spread of cancer cells [56-58]. It is a multifunctional protein that interacts with several other proteins with many functions under various pathophysiological conditions [59]. For example, VIM interacts with the insulin-like growth factor 1 receptor, promotes axonal extension, and serves as a double-edged sword in the nervous system by regulating axonal regeneration, myelination, apoptosis, and neuroinflammation [60]. Furthermore, *Vim* knockout mice were less susceptible to bacterial infections and had a reduced inflammatory response than wild-type mice [61]. Recently, *Vim* deficiency was shown to prevent obesity and insulin resistance in type 2 DM by reducing CD36 expression on plasma membranes and intracellular trafficking of glucose transporter type 4 in adipocytes [62]. Therefore, the combination of LBH with CRYAB and VIM could improve neurovascular regeneration in diabetic ED by activating the angiogenic effects of CRYAB and potentially reducing the inflammatory effects of VIM. Further studies are required to better understand the exact regulatory mechanisms underlying the effects of LBH and its binding partners.

Methods

Ethics statement and animal treatment

Eight-week-old male C57BL/6 mice (Orient Bio, Seongnam-si, Gyeonggi-do, Korea) were used in this study. Animal experiments were approved by the Institutional Animal Care and Use Subcommittee of Inha university (**IACUC approval number: 200910-719**). All tissue donors provided informed consent, and the experiments were approved by the Ethics Committee and the internal review board of Inha University (**IRB No. 2007-730**). Animals were monitored daily for health and behavior as previous studies described [8,63]. Briefly, mice were maintained at room temperature (RT) (23 ± 2˚C), 40-60% relative humidity, 12 hours light/dark cycle, and specific pathogen-free conditions. Sixty adult male C57BL/6 mice were used for single cell sequencing analysis, mouse cavernous pericyte culture (*in vitro* study), and erectile function evaluation (*in vivo* study). All animals were anesthetized with intramuscular injections of ketamine (100 mg/kg, Yuhan Corp., Seoul, Korea) and xylazine (5 mg/kg, Bayer Korea, Seoul, Korea). Animals were euthanized by 100% CO_2 gas exchange in a closed container at a CO_2 exchange rate of 10-30% container volume/min. Diabetes mellitus (DM) was induced as described previously. Shortly, low doses of streptozotocin (STZ, 50 mg/kg, i.p., Sigma-Aldrich, St. Louis, MO, USA) was injected for 5 consecutive days. Eight weeks later, only mice with a tail vein blood glucose level higher than 300 mg/dL and significantly decreased body weights were considered to have DM. Fasting and postprandial blood glucose levels were determined using an Accu-Check blood glucose meter (Roche Diagnostics, Mannheim, Germany) before starting all *in vivo* studies. No mice died during erectile function evaluation experiment, and all experiments were performed in a blinded manner.

To test the efficacy of LBH on erectile function, the mice were distributed into four groups as follows: control nondiabetic mice (n = 5) and mice with STZ-induced diabetes receiving one successive intracavernous injections of phosphate-buffered saline (n = 5, PBS, 20 μL), lentiviruses ORF control particles (n = 5, NC, $5x10^4$ infection units in 20 μL; Origene Technology, Rockville, MD, USA) or lentiviruses containing ORF mouse clone of LBH (n = 5, LBH O/E, $5x10^4$ infection units in 20 μL; Origene Technology) into the midportion of the corpus cavernosum. A vascular clamp was used to pressurize the bottom of penises immediately before injection and was left in place for 30 minutes to restrict blood outflow.

Single cell RNA sequencing

After mice were euthanized, the penis tissues (n = 5 for each group) were harvested, minced and digested using Multi Tissue dissociation kit (Miltenyi, 130-110-201) with minor modifications as described previously [64]. Briefly, tissues were homogenized using 21G and 26 1/2 G syringes. The tissues were digested with 50 µL of Enzyme D, 25 µL of Enzyme R and 6.75 µL of Enzyme A in 500 µL of DMEM and incubated for 10 minutes at 37 ˚C. The enzymes were deactivated by 10% FBS and solution was then passed through tip strainer (70 µm and then 40 µm). After centrifugation at 1,000 RPM for 5 minutes, cell pellet was incubated with 1 ml of RBC lysis buffer on ice for 3 minutes. After the cell number and viability were analyzed by using Countess AutoCounter (Invitrogen, C10227), the single cell suspension was loaded onto 10x Chromium Single Cell instrument (10x Genomics). Barcoding and cDNA synthesis were performed according to the manufacturer's instructions.

Quality control, clustering, and cell type annotation

FASTQ files from sequencing were aligned to the mouse reference sequence (mm10) using CellRanger count pipeline (10x Genomics, Version 3.0.2). Filtered feature-barcode matrices outputs by CellRanger were used to create Seurat objects for single cell RNA sequencing data analysis (Seurat v3.1.5). Cells with the number of genes less than 200 were filtered out from Seurat objects. Quality controlled data were normalized using NormalizeData function with default parameters. Highly variable features were identified using the FindVariableFeatures function with default parameters. Data were scaled by setting the number of UMI as variables to regress out using ScaleData function. The scaled data were merged into one Seurat object, and then normalized, and highly variable genes were identified and scaled. Linear dimensional reduction performed using RunPCA function with 30 principal components. The RunHarmony function was used to correct the batch effect between the merged data. Cells were clustered based on similar feature expression patterns using FindClusters function (resolution = 1.5) and FindNeighbors (reduction = "harmony", dims = 1:20). To visualize and explore data, non-linear dimensional reduction was performed using Uniform Manifold Approximation and Projection (UMAP). To merge clusters with similar gene expression patterns, FindMarkers function (test.use = ‘bimod’) parameters was used to find differentially expressed genes (DEGs), and cluster pairs with less than 10 DEGs (adjusted p-value < 0.01, log_fold change ≥ 1) were merged. DEGs of each cluster were found using FindAllMarkers function (max.cells.per.ident = 100, min.diff.pct = 0.3, only.pos = TRUE).

The clusters were annotated by expression of marker genes (*Comp* and *Fn1* for Chondrocytes; *Col1a1*, *Col1a2* and *Fbln1* for Fibroblasts; *Mylk* and *Col3a1* for Fibrochondrocytes progenitor; *Prg4* and *Anxa8* for

differentiating fibrochondrocyte; *Mgp* and *Mfap5* for reticular fibroblast; *C7*, *Lum* and *Mmp2* for Myofibroblast; *Prox1*, *Ccl21a* and *Lyve1* for Lymphatic endothelial cell; *Foxc2* for valve-related lymphatic endothelial cell; *Eng* and *Flt1* for vascular endothelial cell; *Cnn1* for smooth muscle cell; *Rgs5* for Pericyte; *Cadm4* and *Plp1* for Schwann cell; *Cd68*, *C1qa* and *C1qb* for Macrophage).

Identification of differential expressed genes and gene ontology analysis

DEGs between two groups were identified using FindMarkers function (test.use = 'MAST') from Seurat R package. Among the DEGs found by FindMarkers based on bonferroni correction, only genes with |log_fold change| > 0.25 and adjusted p-value < 0.05 were considered as significant DEGs. DEGs were visualized as volcano plots. Gene ontology analysis was performed using DAVID with significant DEGs as inputs. Gene ontology analysis on molecules of the protein-protein interaction network included parent terms (GOTERM_BP_5), and the others were gene ontology mappings directly annotated by the source database (GOTERM_BP_DIRECT). Only terms with p-value < 0.05 and FDR < 0.25 were considered significant gene ontology.

Gene set enrichment analysis (GSEA)

Enriched gene sets between two groups were identified using GSEA (http://www.broadinstitute.org/gsea/index.jsp) with 1000 gene set permutation. Curated (c2), ontology (c5) gene sets and hallmarks (h) gene sets were selected as gene sets database. A 'Signal2Noise' metric was used for ranking genes, and gene sets larger than 500 or smaller than 5 were excluded from the analysis. Only gene sets with p-value < 0.05 and false discovery rate < 0.25 were considered significant enriched gene sets.

Single cell gene regulatory network analysis

Transcription factor (TF) activity of normal or diabetic pericyte were identified using SCENIC R package (v1.1.2-01). To avoid narrow comparison of TF activity in pericytes between normal and diabetic conditions that could lead to faulty reasoning, we included SMCs in the comparison as well. Raw count matrices of SMC and Pericyte extracted from the Seurat object were used as input for SCENIC. 10 kb around the transcription start site (TSS) and 500 bp upstream of the TSS were selected for motif ranking. Genes in input matrix were filtered using geneFiltering function with default parameters. To split targets into positive and negative correlated targets,

the correlation was calculated using runCorrelation function. Potential transcription factor targets were inferred using runGenie3 function. Building and scoring the gene regulatory network were performed using runSCENIC functions. Clustering and dimensionality reduction on the regulon activity were performed using tsneAUC function. Only angiogenesis-related TFs with differences in activity between normal and diabetic pericytes were visualized in the heatmap.

Single cell data of human corpus cavernosum analysis

To determine whether *LBH* could also be a marker of pericyte in human, we analyzed single cell RNA data of human corpus cavernosum from previous study [38]. Quality control was performed according to method of previous study. Quality controlled data were processed according to our data analysis methods. Cells were clustered using FindClusters function (resolution = 0.5). The DEGs of three clusters expressing the SMC markers *ACTA2* and *MYH11*, used in the previous study, were found with the FindAllMarker function. We defined significant DEGs as genes with log_fold change > 0.25, adjusted p-value < 0.05, and non-overlapping DEGs in different clusters. These significant DEGs were used for gene ontology analysis for cell type identification.

Cell-cell interaction analysis

Ligand-receptor communications between cell types were predicted using CellPhoneDB (https://github.com/Teichlab/cellphonedb) and CellChat (https://github.com/sqjin/CellChat). Normalized single cell data was used as input for analysis. We performed CellPhoneDB with the statistical method. Interactions that did not differ by more than 0.25-fold mean values between diabetes and normal were considered to have no significant difference. Even if there is a difference in the mean value between diabetes and normal, interactions with p-value of 1 in both diabetes and normal were considered insignificant. The outputs of CellPhoneDB were visualized using ktplot in R. CellChat was performed according to tutorial for comparison analysis of multiple datasets with different cell type compositions.

Protein-protein interaction (PPI) network visualization

PPIs of LBH, CRYAB, VIM, and 1st and 2nd interactors of LBH were found by BioGRID and STRING database (Organisms: Mus musculus). In the STRING database, textmining, experiments, and databases were used as

active interaction sources, and only interactions with a minimum required interaction score higher than 0.7 were identified. The identified PPIs were visualized using Cytoscape [38].

Cell culture

Mouse aortic smooth muscle cells (Aorta SMC; CRL-2797, ATCC) and human pericytes from placenta (hPC-PL; C-12980, PromoCell) were authenticated according to ATCC and PromoCell guidelines and used within 6 months of receipt. Aorta SMC and hPC-PL were cultured in complement Dulbecco's modified Eagle Medium (DMEM; Gibco, Carlsbad, CA, USA) supplemented with 10% FBS, and 1% penicillin/streptomycin (Gibco), and incubated the cells at 37°C in a 5% CO_2 atmosphere.

For the primary culture of mouse cavernous pericytes (MCPs), followed the protocol described previously, in brief, the cavernous tissue was cut into several pieces around 1 mm, and the pieces settled by gravity to the collagen I-coated 35-mm cell culture dishes (BD Biosciences). After 30 min incubation at 37°C with 300 µL complement of DMEM, 10% FBS, 1% penicillin/streptomycin, and 10 nM human pigment epithelium-derived factor (PEDF; Sigma- Aldrich), we added an additional 900 µL complement medium and incubated the samples at 37°C in a 5% CO2 atmosphere. Change the medium every 2 days. After the cells are confluent and spread to the bottom of the dish (approximately 2 weeks after the start of culture), subculture using only sprouting cells. The sprouting cells were seeded onto dishes coated with 50 µL/ml collagen I (Advanced BioMatrix). Cells between passages 2 and 4 were used for experiments. In order to examine the effect of LBH overexpression under normal glucose (NG, 5mM glucose, Sigma-Aldrich) or high glucose (HG, 30 mM glucose, Sigma-Aldrich) conditions, MCPs were infected with lentiviruses ORF control particles (NC, $5x10^5$ infection units per millilitre cultured medium; Origene Technology) or ORF clone of mouse LBH (LBH O/E, $5x10^5$ infection units per millilitre cultured medium; Origen Technology) under high glucose conditions for at least 3 days.

Human corpus cavernosum tissue and cavernous pericyte culture

For fluorescence examinations, human corpus cavernosum tissues were obtained from two patients with congenital penile curvature (59-year-old and 47-year-old) who had normal erectile function during reconstructive penile surgery and two patients with diabetic ED (69-year-old and 56-year-old) during penile prosthesis implantation. For primary pericyte culture, the fresh adult corpus cavernosum tissues from patients (59-year-old) with congenital penile curvature who have normal erectile function during reconstructive penile

surgery were collected after surgery and transferred into sterile vials containing Hank's balanced salt solution (GIBCO, Carlsbad, CA, USA) and washed twice in PBS. The detailed methods of the human cavernous pericytes were isolated and maintained as described previously [16,65]. Human cavernous pericytes at passages 2 or 3 were used for experiments. All tissue donors provided informed consent, and the experiments were approved by the internal review board of our university.

Measurement of Erectile Function

Erectile function was measured after mice were anesthetized by intraperitoneal injection of ketamine (100 mg/kg) and xylazine (5 mg/kg) as described previously. Briefly, the cavernous nerve was stimulated for 1 minute using bipolar platinum wire electrodes at 1 or 5 V at 12 Hz and a pulse width of 1 ms condition. Each stimulation was repeated at least 2 times every 10 minutes. Record the maximal intracavernous pressure (ICP) and total ICP during stimulation. The area under the curve (AUC) from the initiation of cavernous nerve stimulation to 20 seconds after stimulation termination was measured as total ICP. Before ICP measurements, the systemic blood pressure was measured continuously using a noninvasive tail-cuff system (Visitech Systems, Apex, NC, USA). The ratio of maximal ICP and total ICP to mean systolic blood pressure (MSBP) was calculated to normalize variations in systemic blood pressure.

TUNEL Assay

The MCPs cell death after infected with lentiviruses ORF control particles (NC, $5x10^4$ infection units per millilitre cultured medium; Origene Technology) or ORF clone of mouse LBH (LBH O/E, $5x10^4$ infection units per millilitre cultured medium; Origen Technology) under NG or HG conditions were evaluated by TUNEL (terminal deoxynucleotidyl transferase-mediated deoxyuridine triphosphate nick-end labeling) assay using the ApopTag® Fluorescein In Situ Apoptosis Detection Kit (S7160, Chemicon, Temecula, CA, USA) according to the manufacturer's instructions. Numbers of TUNEL-positive apoptotic cells were obtained by a confocal fluorescence microscope.

Cell migration assay

MCPs migration assays were performed using the SPLScar™Block system (SPL life sciences, Pocheon-si, Gyeonggi-do, Korea) on 60-mm culture dishes. In brief, MCPs was infected with lentiviruses ORF control

particles (NC, $5x10^4$ infection units per millilitre cultured medium; Origene Technology) or ORF clone of mouse LBH (LBH O/E, $5x10^4$ infection units per millilitre cultured medium; Origen Technology) under NG or HG conditions. Then conditioned cells were seeded into 3-well blocks at >90% confluence. Blocks were removed after 5 hours and cells were incubated for additional 24 hours in DMEM medium containing 2% FBS and thymidine (2 mM, Sigma-Aldrich). The images were taken using a phase-contrast microscope (Olympus), and cell migration was analyzed by determining the percentage of cells that moved into the frame line showed in the figures from four separate block systems in a blinded manner using Image J software (National Institutes of Health [NIH] 1.34, http://rsbweb.nih.gov/ij/).

***In vitro* tube formation assay**

Tube formation assay was performed as described previously [63]. The assay was performed in a CO_2 incubator and the images were obtained at 24 hours at a screen magnification of 40 with a phase-contrast microscope (CKX41, Olympus, Japan) and the numbers of master junctions from four separate experiments was determined by using Image J software.

***Ex vivo* neurite sprouting assay**

Major pelvic ganglion (MPG) tissues were harvested and maintained as described previously [8]. After the tissue was covered with matrigel and incubated at 37 °C for 10 minutes in a 5% CO_2 atmosphere, followed by incubation in 1.2 ml of complete Neurobasal medium (Gibco) containing 0.5 nM GlutaMAX™-I (Gibco) and 2% serum-free B-27 (Gibco). The MPG tissues were infected with lentiviruses ORF control particles (NC, $5x10^4$ infection units per millilitre cultured medium; Origene Technology) or ORF clone of mouse LBH (LBH O/E, $5x10^4$ infection units per millilitre cultured medium; Origen Technology) under NG or HG conditions. Five days later, neurite outgrowth segments were then fixed in 4% paraformaldehyde for at least 30 minutes and immunofluorescence staining with an anti-neurofilament antibody (N4142; Sigma-Aldrich; 1:50).

Proteome profiler Mouse angiogenesis array analysis

Secreted angiogenesis factors in cavernous tissue between normal and diabetes condition were detected using a proteome profiler mouse angiogenesis array kit (ARY015; R&D Systems Inc.), as described by the manufacturer. This array detects 53 mouse angiogenesis-related protein simultaneously. The intensity of dot blots was

analyzed using Image J software.

Histological examination

For fluorescence examinations, tissues were fixed in 4% paraformaldehyde overnight at 4°C, and cell samples were fixed in 4% paraformaldehyde for 15 minutes at RT. After blocking with 1% BSA (Sigma-Aldrich) for 1 hour at RT, frozen tissue sections (12-μm as thick) or cell samples were incubated with primary antibodies at 4°C overnight. The antibodies used were as follows: anti-LBH (1:200; Novus Biologicals, Littleton, CO, USA), anti-CD31 antibody (1:50; Millipore), anti-PDGFR□ (1:100; Invitrogen), anti-α-SMA (1:100; Abcam, Cambridge, MA, USA), anti-CD140b (1:100; Invitrogen), anti-NG2 antibody (1:100; Millipore), anti-Neurofilament (1:100; Sigma-Aldrich), neuronal nitric oxide synthase (nNOS; 1:50; Santa Cruz Biotechnology, Dallas, TX, USA), anti-phospho-HistoneH3 (1:50; Millipore; 1:50), anti-vimentin (1:100; Sigma-Aldrich), and anti-Crystallin Alpha B (CRYAB, 1:100; Invitrogen). Washes the samples with PBS (Gibco) for at least 3 times, tissue sections or cell samples were incubated with donkey anti-rabbit DyLight® 550 (1:200; Abcam), donkey anti-mouse Alexa Fluor® 488 (1:200; Jackson ImmunoResearch Laboratories, West grove, PA, USA), goat anti-Armenian hamster Fluorescein (FITC) (1:200; Jackson ImmunoResearch Laboratories), and donkey anti-chicken rhodamine (TRITC) secondary antibodies (1:200; Jackson ImmunoResearch Laboratories) for 2 hours at room temperature. Samples were mounted with a solution containing 4,6-diamidino-2-phenylindole (DAPI [H-1200, Vector Laboratories Inc., Burlingame, CA, USA]) for nuclei staining. All images were obtained using a confocal microscope (K1-Fluo; Nanoscope Systems, Inc.). Quantitative analysis was performed using Image J software (National Institutes of Health [NIH] 1.34, http://rsbweb.nih.gov/ij/).

LC-MS/MS analysis of immunoprecipitates

The LC-MS/MS analysis was performed as a custom service by Yonsei Proteome Research Center (Yonsei Proteome Research Center, Seoul, Republic of Korea) as previously described. In brief, total cell lysates were immunoprecipitated with LBH antibody (1:50; Sigma-Aldrich), and analyzed by SDS-PAGE and Coomassie Blue staining. The indicated bands (**Fig. 6**, framed in red dot line) were excised from SDS-PAGE gels, and Nano LC-MS/MS analyses were performed using an Easy n-LC (Thermo Fisher, San Jose, CA, USA) and an LTQ Orbitrap XL mass spectrometer (Thermo Fisher) equipped with a nano-electrospray source [66]. Samples were

separated on a C18 nanobore column (150 mm × 0.1 mm, 3 μm pore size; Agilent). Mobile phase A for LC separation was 0.1% formic acid plus 3% acetonitrile in deionized water and mobile phase B was 0.1% formic acid in acetonitrile. The chromatography gradient was designed to achieve a linear increase from 0% B to 32% B in 23 minutes, 32% B to 60% B in 3 minutes, 95% B in 3 minutes, and 0% B in 6 minutes. The flow rate was maintained at 1500 nl/min. Mass spectra were acquired using data-dependent acquisition with a full mass scan (350–1800 m/z) followed by 10 MS/MS scans. For MS1 full scans, the orbitrap resolution was 15,000 and the AGC was 2×10^5. For MS/MS in the LTQ, the AGC was 1×10^4. The Mascot algorithm (Matrix Science, USA) was used to identify peptide sequences present in a protein sequence database. Database search criteria were as follows: taxonomy, Homo sapiens, Mus musculus; fixed modification, carbamidomethylated at cysteine residues; variable modification, oxidized at methionine residues; maximum allowed missed cleavages, 2; MS tolerance, 10 ppm; MS/MS tolerance, 0.8 Da. Only peptides resulting from trypsin digests were considered. Peptides were filtered with a significance threshold of $P < 0.05$.

Immunoblots and Immunoprecipitation

Cells and tissues were lysed in RIPA buffer (Sigma-Aldrich) supplemented with protease (GenDEPOT, LLC, Katy, TX, USA) and phosphatase (GenDEPOT, LLC) inhibitors. Equal amounts of proteins (30 μg per lane) from whole-cell or tissue lysates were resolved by SDS-PAGE on 8% to 15% gels, and then transferred to polyvinylidene fluoride (PVDF) membranes. After blocking with 5% non-fat dried milk for 1 hour at RT, membranes were incubated at 4°C overnight with the following primary antibodies: anti-LBH (1:1000; Sigma-Aldrich), anti-Vimentin (1:1000; Sigma-Aldrich), and anti-CRYAB (1:1000; Invitrogen). For immunoprecipitation, 1,000 μg of lysate was incubated with the indicated antibody (1–2 μg) for 3–4 hours at 4°C followed by overnight incubation with Protein A/G PLUS-Agarose (Santa Cruz Biotechnology). Immunoprecipitates were washed five times with RIPA buffer, and then were resolved by SDS–PAGE and immunoblotted with the indicated antibodies. Densitometric analyses of Western blot bands were performed using Image J software (National Institutes of Health [NIH] 1.34, http://rsbweb.nih.gov/ij/).

Statistical analysis

Results are expressed as the means ± SEMs of at least four independent experiments. The unpaired t test was used to compare two groups, and One-way ANOVA followed by Tukey's post hoc test for four-group

comparisons. The analysis was conducted using GraphPad Prism version 8 (GraphPad Software, Inc., La Jolla, CA, USA, www.graphpad.com), and statistical significance was accepted for P values <0.05.

Author contributions

Seo-Gyeong Bae

School of Life Sciences, Gwangju Institute of Science and Technology, 123 Cheomdangwagi-ro, Buk-gu, Gwangju, Republic of Korea

Contribution: Data analysis, Writing - original draft, Writing - review and editing

Competing interests: No competing interests declared

Guo Nan Yin

National Research Center for Sexual Medicine and Department of Urology, Inha University School of Medicine, 100 Inha-ro, Michuhol-gu, Incheon, Republic of Korea

Contribution: Performing experiments, Writing - original draft, Writing - review and editing

Competing interests: No competing interests declared

Jiyeon Ock

National Research Center for Sexual Medicine and Department of Urology, Inha University School of Medicine, 100 Inha-ro, Michuhol-gu, Incheon, Republic of Korea

Contribution: Performing experiments, Writing - review and editing

Competing interests: No competing interests declared

Jun-Kyu Suh, MD, PhD

National Research Center for Sexual Medicine and Department of Urology, Inha University School of Medicine, 100 Inha-ro, Michuhol-gu, Incheon, Republic of Korea

Contribution: Funding acquisition, Conceptualization, Writing - review and editing

For correspondence: jksuh@inha.ac.kr

Competing interests: No competing interests declared

Ji-Kan Ryu, MD, PhD

National Research Center for Sexual Medicine and Department of Urology, Inha University School of Medicine, 100 Inha-ro, Michuhol-gu, Incheon, Republic of Korea

Contribution: Funding acquisition, Conceptualization, Writing - review and editing

For correspondence: rjk0929@inha.ac.kr

Competing interests: No competing interests declared

Jihwan Park, PhD

School of Life Sciences, Gwangju Institute of Science and Technology, 123 Cheomdangwagi-ro, Buk-gu, Gwangju, Republic of Korea

Contribution: Funding acquisition, Conceptualization, Data analysis direction, Writing - original draft, Writing - review and editing

For correspondence: jihwan.park@gist.ac.kr.

Competing interests: No competing interests declared

Data availability

The raw data was deposited in Korean Nucleotide Archive (KoNA, https://kobic.re.kr/kona) with the accession ID, PRJKA230548. All data associated with this study are available in the main text or the supplementary materials.

Acknowledgements

This work was funded by the National Research Foundation of Korea (NRF) grants (Guo Nan Yin, NRF-2021R1A2C4002133, Ji-Kan Ryu, 2022R1A2B5B02001671, Jihwan Park, 2019R1C1C1005403 and 2021M3H9A2097520), and a Medical Research Center grant (Ji-Kan Ryu, NRF-2021R1A5A2031612) funded by the Korean government. This work was also supported by the 2023 GIST-MIT Research Collaboration grant funded by the GIST.

References

1 Kubin, M., Wagner, G. & Fugl-Meyer, A. R. Epidemiology of erectile dysfunction. *International journal of impotence research* **15**, 63-71 (2003).

2 Ayta, I., McKinlay, J. & Krane, R. The likely worldwide increase in erectile dysfunction between 1995 and 2025 and some possible policy consequences. *BJU international* **84**, 50-56 (1999).

3 Kessler, A., Sollie, S., Challacombe, B., Briggs, K. & Van Hemelrijck, M. The global prevalence of erectile dysfunction: a review. *BJU international* **124**, 587-599 (2019).

4 Sáenz de Tejada, I. i., Anglin, G., Knight, J. R. & Emmick, J. T. Effects of tadalafil on erectile dysfunction in men with diabetes. *Diabetes care* **25**, 2159-2164 (2002).

5 Bivalacqua, T. J., Usta, M. F., Champion, H. C., Kadowitz, P. J. & Hellstrom, W. J. Endothelial dysfunction in erectile dysfunction: role of the endothelium in erectile physiology and disease. *Journal of Andrology* **24**, S17-S37 (2003).

6 Miner, M. M. Erectile dysfunction: a harbinger or consequence: does its detection lead to a window of curability? *Journal of andrology* **32**, 125-134 (2011).

7 Angulo, J. *et al.* Diabetes exacerbates the functional deficiency of NO/cGMP pathway associated with erectile dysfunction in human corpus cavernosum and penile arteries. *The journal of sexual medicine* **7**, 758-768 (2010).

8 Ghatak, K. *et al.* Heat Shock Protein 70 in Penile Neurovascular Regeneration Requires Cystathionine Gamma-Lyase. *The World Journal of Men's Health* **40**, 580-599 (2022).

9 Anita, L. *et al.* Pericyte-derived extracellular vesicle-mimetic nanovesicles ameliorate erectile dysfunction via lipocalin 2 in diabetic mice. *International Journal of Biological Sciences* **18**, 3653-3667 (2022).

10 Yin, G. N. *et al.* Transcriptional profiling of mouse cavernous pericytes under high-glucose conditions: Implications for diabetic angiopathy. *Investigative and Clinical Urology* **62**, 100 (2021).

11 Gerhardt, H. & Betsholtz, C. Endothelial-pericyte interactions in angiogenesis. *Cell Tissue Res.* **314**, 15-23 (2003).

12 Liu, Y. *et al.* Reduced pericyte and tight junction coverage in old diabetic rats are associated with hyperglycemia-induced cerebrovascular pericyte dysfunction. *American Journal of Physiology-Heart and Circulatory Physiology* **320**, H549-H562 (2021).

13 Warmke, N., Griffin, K. J. & Cubbon, R. M. Pericytes in diabetes-associated vascular disease. *Journal of Diabetes and its Complications* **30**, 1643-1650 (2016).

14 Shimizu, F., Sano, Y., Haruki, H. & Kanda, T. Advanced glycation end-products induce basement membrane hypertrophy in endoneurial microvessels and disrupt the blood–nerve barrier by stimulating the release of TGF-β and vascular endothelial growth factor (VEGF) by pericytes. *Diabetologia* **54**, 1517-1526 (2011).

15 Yin, G. N. *et al.* The pericyte as a cellular regulator of penile erection and a novel therapeutic target for erectile dysfunction. *Scientific Reports* **5**, 10891 (2015).

16 Kim, M. *et al.* A simple and nonenzymatic method to isolate human corpus cavernosum endothelial cells and pericytes for the study of erectile dysfunction. *The World Journal of Men's Health* **38**, 123-131 (2020).

17 Reddy, M. A. *et al.* Regulation of vascular smooth muscle cell dysfunction under diabetic conditions by miR-504. *Atertio. Thromb. Vasc. Biol.* **36**, 864-873 (2016).

18 Wei, A. *et al.* Characterization of corpus cavernosum smooth muscle cell phenotype in diabetic rats with erectile dysfunction. *International journal of impotence research* **24**, 196-201 (2012).

19 Kumar, A. *et al.* Specification and diversification of pericytes and smooth muscle cells from mesenchymoangioblasts. *Cell reports* **19**, 1902-1916 (2017).

20 Smyth, L. C. *et al.* Markers for human brain pericytes and smooth muscle cells. *J. Chem. Neuroanat.* **92**, 48-60 (2018).

21 Chasseigneaux, S. *et al.* Isolation and differential transcriptome of vascular smooth muscle cells and mid-capillary pericytes from the rat brain. *Scientific Reports* **8**, 12272 (2018).

22 Sun, Y. *et al.* A Single-Cell Survey of Cellular Heterogeneity in Human Great Saphenous Veins. *Cells* **11**, 2711 (2022).

23 Baek, S.-H. *et al.* Single cell transcriptomic analysis reveals organ specific pericyte markers and identities. *Frontiers in Cardiovascular Medicine* **9** (2022).

24 Ismail, E., Younis, S., Ismail, I., El-Wazir, Y. & El-Sakka, A. Early administration of phosphodiesterase 5 inhibitors after induction of diabetes in a rat model may prevent erectile dysfunction. *Andrology* **8**, 241-248 (2020).
25 Abdelbaky, T. M., Brock, G. B. & Huynh, H. Improvement of erectile function in diabetic rats by insulin: possible role of the insulin-like growth factor system. *Endocrinology* **139**, 3143-3147 (1998).
26 Sullivan, C. J. *et al.* Microarray analysis reveals novel gene expression changes associated with erectile dysfunction in diabetic rats. *Physiol. Genomics* (2005).
27 Kowalczyk, A., Kleniewska, P., Kolodziejczyk, M., Skibska, B. & Goraca, A. The role of endothelin-1 and endothelin receptor antagonists in inflammatory response and sepsis. *Archivum immunologiae et therapiae experimentalis* **63**, 41-52 (2015).
28 Guo, M., Zhang, H., Zheng, J. & Liu, Y. Glypican-3: a new target for diagnosis and treatment of hepatocellular carcinoma. *Journal of Cancer* **11**, 2008 (2020).
29 Wittrisch, S. *et al.* NPY1R-targeted peptide-mediated delivery of a dual PPARα/γ agonist to adipocytes enhances adipogenesis and prevents diabetes progression. *Molecular Metabolism* **31**, 163-180 (2020).
30 Haghighi, K., Bidwell, P. & Kranias, E. G. Phospholamban interactome in cardiac contractility and survival: A new vision of an old friend. *Journal of Molecular and Cellular Cardiology* **77**, 160-167 (2014).
31 Dai, J. *et al.* Osteopontin induces angiogenesis through activation of PI3K/AKT and ERK1/2 in endothelial cells. *Oncogene* **28**, 3412-3422 (2009).
32 Browne, S. *et al.* TGF-β1/CD105 signaling controls vascular network formation within growth factor sequestering hyaluronic acid hydrogels. *PLoS One* **13**, e0194679 (2018).
33 Li, T. *et al.* IGFBP2: integrative hub of developmental and oncogenic signaling network. *Oncogene* **39**, 2243-2257 (2020).
34 Lin, C. G. *et al.* CCN3 (NOV) is a novel angiogenic regulator of the CCN protein family. *J. Biol. Chem.* **278**, 24200-24208 (2003).
35 Kyriakides, T. R., Hartzel, T., Huynh, G. & Bornstein, P. Regulation of angiogenesis and matrix remodeling by localized, matrix-mediated antisense gene delivery. *Mol. Ther.* **3**, 842-849 (2001).
36 Abdul, Y., Jamil, S., Li, W. & Ergul, A. Cerebral microvascular matrix metalloproteinase-3 (MMP3) contributes to vascular injury after stroke in female diabetic rats. *Neurochem. Int.* **162**, 105462 (2023).
37 Jiang, Y. *et al.* Overexpression of Limb-Bud and Heart (LBH) promotes angiogenesis in human glioma via VEGFA-mediated ERK signalling under hypoxia. *EBioMedicine* **48**, 36-48 (2019).
38 Zhao, L. *et al.* Single-cell transcriptome atlas of the human corpus cavernosum. *Nature communications* **13**, 4302 (2022).
39 Pourhaghighi, R. *et al.* BrainMap elucidates the macromolecular connectivity landscape of mammalian brain. *Cell systems* **10**, 333-350. e314 (2020).
40 Desai, A., Chen, R., Cayetano, A., Jayasena, C. N. & Minhas, S. Understanding and treating ejaculatory dysfunction in men with diabetes mellitus. *Andrology* **11**, 379-398 (2023).
41 Burchardt, M. *et al.* Application of angiogenic factors for therapy of erectile dysfunction: protein and DNA transfer of VEGF 165 into the rat penis. *Urology* **66**, 665-670 (2005).
42 Jin, H.-R. *et al.* Intracavernous delivery of a designed angiopoietin-1 variant rescues erectile function by enhancing endothelial regeneration in the streptozotocin-induced diabetic mouse. *Diabetes* **60**, 969-980 (2011).
43 Yin, G. N. *et al.* Pericyte-derived Dickkopf2 regenerates damaged penile neurovasculature through an angiopoietin-1-Tie2 pathway. *Diabetes* **67**, 1149-1161 (2018).
44 Yin, G. N. *et al.* Latrophilin-2 is a novel receptor of LRG1 that rescues vascular and neurological abnormalities and restores diabetic erectile function. *Experimental & Molecular Medicine* **54**, 626-638 (2022).
45 Hu, L., Qi, S., Zhang, K. & Fu, Q. Essential role of brain-derived neurotrophic factor (bdnf) in diabetic erectile dysfunction. *Andrologia* **50**, e12924 (2018).
46 Bennett, N. E. *et al.* Improvement in erectile dysfunction after neurotrophic factor gene therapy in diabetic rats. *The Journal of urology* **173**, 1820-1824 (2005).
47 Birbrair, A. *et al.* Pericytes at the intersection between tissue regeneration and pathology. *Clinical science* **128**, 81-93 (2015).
48 Briegel, K. J. & Joyner, A. L. Identification and characterization of Lbh, a novel conserved nuclear protein expressed during early limb and heart development. *Dev. Biol.* **233**, 291-304 (2001).

49 Rieger, M. E., Sims, A. H., Coats, E. R., Clarke, R. B. & Briegel, K. J. The embryonic transcription cofactor LBH is a direct target of the Wnt signaling pathway in epithelial development and in aggressive basal subtype breast cancers. *Mol. Cell. Biol.* **30**, 4267-4279 (2010).
50 Powder, K. E., Cousin, H., McLinden, G. P. & Craig Albertson, R. A nonsynonymous mutation in the transcriptional regulator lbh is associated with cichlid craniofacial adaptation and neural crest cell development. *Mol. Biol. Evol.* **31**, 3113-3124 (2014).
51 Wu, A. *et al.* Exosomal LBH inhibits epithelial-mesenchymal transition and angiogenesis in nasopharyngeal carcinoma via downregulating VEGFA signaling. *International Journal of Biological Sciences* **18**, 242 (2022).
52 Wu, A. *et al.* Limb-bud and heart (LBH) inhibits cellular migration, invasion and epithelial-mesenchymal transition in nasopharyngeal carcinoma via downregulating αB-crystallin expression. *Cell. Signal.* **85**, 110045 (2021).
53 Zacchigna, S., Lambrechts, D. & Carmeliet, P. Neurovascular signalling defects in neurodegeneration. *Nature Reviews Neuroscience* **9**, 169-181 (2008).
54 Dimberg, A. *et al.* αB-crystallin promotes tumor angiogenesis by increasing vascular survival during tube morphogenesis. *Blood, The Journal of the American Society of Hematology* **111**, 2015-2023 (2008).
55 Guo, M. *et al.* The role of vimentin intermediate filaments in cortical and cytoplasmic mechanics. *Biophys. J.* **105**, 1562-1568 (2013).
56 Dave, J. M. & Bayless, K. J. Vimentin as an integral regulator of cell adhesion and endothelial sprouting. *Microcirculation* **21**, 333-344 (2014).
57 Chen, Z., Fang, Z. & Ma, J. Regulatory mechanisms and clinical significance of vimentin in breast cancer. *Biomedicine & Pharmacotherapy* **133**, 111068 (2021).
58 Liu, C.-Y., Lin, H.-H., Tang, M.-J. & Wang, Y.-K. Vimentin contributes to epithelial-mesenchymal transition cancer cell mechanics by mediating cytoskeletal organization and focal adhesion maturation. *Oncotarget* **6**, 15966 (2015).
59 Danielsson, F., Peterson, M. K., Caldeira Araújo, H., Lautenschläger, F. & Gad, A. K. B. Vimentin diversity in health and disease. *Cells* **7**, 147 (2018).
60 Chen, K.-Z. *et al.* Vimentin as a potential target for diverse nervous system diseases. *Neural Regeneration Research* **18**, 969-975 (2023).
61 Moisan, E., Chiasson, S. & Girard, D. The intriguing normal acute inflammatory response in mice lacking vimentin. *Clinical & Experimental Immunology* **150**, 158-168 (2007).
62 Luo, H. *et al.* Characterizing dedifferentiation of thyroid cancer by integrated analysis. *Science Advances* **7**, eabf3657 (2021).
63 Yin, G. N. Pericyte-derived heme-binding protein 1 promotes angiogenesis and improves erectile function in diabetic mice. *Investigative and Clinical Urology* **63**, 464-474 (2022).
64 Park, J. *et al.* Single-cell transcriptomics of the mouse kidney reveals potential cellular targets of kidney disease. *Science* **360**, 758-763 (2018).
65 Neng, L. *et al.* Isolation and culture of endothelial cells, pericytes and perivascular resident macrophage-like melanocytes from the young mouse ear. *nature protocols* **8**, 709-720 (2013).
66 Lee, M. J. *et al.* Identification of human complement factor B as a novel biomarker candidate for pancreatic ductal adenocarcinoma. *Journal of proteome research* **13**, 4878-4888 (2014).

Figure Legends

Fig. 1. Single cell transcriptional landscape of mouse cavernous tissues in normal and diabetic conditions. (**A**) Schematic workflow of this study. Cavernous tissues from sixteen-week-old male mice were used for single cell RNA sequencing. DM, diabetes mellitus. (**B**) Visualization of single cell data from mouse cavernous tissues using UMAP. Each cell type is indicated by a different color. FCP, fibrochondrocyte progenitors; FC, fibrochondrocytes; Chond, chondrocytes; FB, fibroblasts; Myo-FB, myofibroblasts; LEC, lymphatic endothelial cells; VEC, vascular endothelial cells; SMC, smooth muscle cells. (**C**) Heatmap of known cell type marker genes used for annotation. (**D**) UMAP projection of four fibroblast clusters and expression of marker genes of four fibroblast subsets. *Egr1* for *Egr1* high FB; *Cxcl12* for *Cxcl12* high FB; *Mgp* for Reticular FB; *Rps25* and *Rps17* for Ribosomal gene high FB. (**E**) Dot plot showing the expression of top five marker genes of each fibroblast subset. (**F**) DEGs between diabetic and normal conditions in Fibroblasts. The top 10 (based on log-fold change) DEGs are indicated with gene names, and genes identified as having high or low expression in diabetes in previous studies are indicated with gene names in red or blue. DEGs with adjusted p-value > 0.05 were indicated in gray. (**G**) Gene ontology analysis of the DEGs higher in normal compared to diabetes in Fibroblasts. (**H**) Gene ontology analysis of the DEGs higher in diabetes compared to normal in Fibroblasts.

Fig. 2. Identification of LBH as a marker of pericytes. (**A**) Expression of well-known marker genes of SMC and Pericyte (*Cnn1* for SMC, *Rgs5* and *Pdgfrb* for Pericyte). (**B**) Significantly enriched gene sets associated with function of SMC and Pericyte. Gene sets with positive normalized enrichment score (NES) are enriched in Pericyte, and negative values are enriched in SMC. (**C**) Violin plots showing expression of *Lbh* in each cell type. (**D**) LBH (red)/a-SMA (green) and LBH (red)/CD31(green) staining in MCPs, aorta SMC, bladder, aorta, and kidney vascular tissues. Nuclei were labeled with DAPI (blue). Scale bars, 25 µm (MCPs and aorta SMC), 50 µm (bladder top panel and kidney vascular) and 100 µm (bladder bottom panel). (**E**) LBH (red)/a-SMA (green) and LBH (red)/PDGFRβ (green) staining in mouse cavernosum, dorsal artery, dorsal vein tissues. Nuclei were labeled with DAPI (blue). Scale bars, 100 µm (cavernosum), 25 µm (dorsal artery) and 50 µm (dorsal vein). Arrows indicate the LBH expressed pericytes. MCPs, mouse cavernous pericytes; SMC, smooth muscle cell; DAPI, 4,6-diamidino-2-phenylindole.

Fig. 3. Cell-cell interactions between pericytes and other cell types in normal and diabetes. (**A**) CellphoneDB dot plots showing angiogenesis-associated ligand-receptor interactions from pericytes to other cell types in normal and diabetic samples. P-values are indicated as circle sizes. The means of the average expression level of the interaction are indicated by color. (**B**) CellphoneDB dot plots showing angiogenesis-associated ligand-receptor interactions from other cell types to pericytes in normal and diabetic samples. P-values are indicated as circle sizes. The means of the average expression level of the interaction are indicated by color. (**C**) The inferred VEGF signaling pathway network in normal and diabetes using CellChat. The width of line represents the communication probability. The color of line matches the sender of the signal. (**D**) GSEA plots showing the gene sets downregulated in diabetic pericytes compared to normal pericytes. (**E**) Heatmap showing the regulon activities of angiogenesis-related transcription factors in pericytes and SMCs in normal and diabetes. (**F**) Proteome profiler mouse angiogenesis array analysis of mouse penis tissues from age-matched control and diabetic mice. The relative expression of each protein was determined by comparing the respective plots to the positive control (reference spot). The frame dot line indicates changed proteins between control and diabetic mice. Expression of the indicated proteins was quantified by assessing the intensity of the dot using Image J. DM, diabetes mellitus.

Fig. 4. LBH improves erectile function under diabetic conditions through induction of neurovascular regeneration. (**A** and **B**) Representative images of immunofluorescence staining of LBH (green)/CD140b (red) in cavernosum tissues and LBH (red) in MCPs under normal and diabetic conditions (*in vivo* and *in vitro*). Nuclei were labeled with DAPI (blue). Scale bar, 100 µm. (**C** and **D**) Quantification of LBH or CD140b expression in *in vivo* and *in vitro* by using Image J, and results are presented as means ± SEM (n = 4). (**E**) Representative western blots for LBH of MCPs under NG and HG conditions, and mouse penis tissues from age-matched control and diabetic mice. (**F**) Normalized band intensity ratio of LBH to β-actin was quantified using Image J, and results are presented as means ± SEM (n = 4). (**G**) Representative intracavernous pressure (ICP) responses for the age-matched control and diabetic mice stimulated at 2 weeks after intracavernous injections with PBS, lentiviruses ORF control particles (NC), and ORF clone of mouse LBH (LBH O/E) (20 µL for PBS, 5 x10^4 IFU/mouse for lentiviral particles). The stimulus interval is indicated by a solid bar. (**H**) Ratios of mean maximal ICP and total ICP (area under the curve) versus MSBP were calculated for each group, and the results are presented as means ± SEM (n = 5). (**I** and **J**) Cavernous CD31 (endothelial cell, red), NG2 (pericyte, green), neurofilament (red), and nNOS (green) staining in cavernous tissues from age-matched control (C) and diabetic mice stimulated at 2 weeks after intracavernous injections with lentiviruses ORF control particles (NC) and ORF clone of mouse LBH (LBH O/E). Scale bars, 100 µm (left), 25 µm (right). (**K-N**) Quantitative analysis of cavernous endothelial cell, pericyte, and neuronal cell content were quantified by Image J, and results are presented as means ± SEM (n = 4). The relative ratio in the NG or control group was defined as 1. **P < 0.01; ***P < 0.001. DM, diabetes mellitus; PBS, phosphate-buffered saline; MCPs, mouse cavernous pericytes; NG, normal glucose; HG, high glucose; DAPI, 4,6-diamidino-2-phenylindole; MSBP, mean systolic blood pressure; ns, not significant.

Fig. 5. LBH as a marker of pericyte in human corpus cavernosum. (**A**) Visualization of single cell data from human corpus cavernosum using UMAP. Each cell type is indicated by a different color. EC, endothelial cell; FB, Fibroblast; SMC, Smooth muscle cell; MFB, Myofibroblast; SWC, Schwann cell; MAC, Macrophage; T, T cell. (**B**) Expression of marker genes of SMC (*ACTA2* and *CNN1*) and marker genes of Pericyte (*RGS5* and *LBH*). (**C**) Biological processes identified through gene ontology analysis of clusters annotated as Pericyte, SMC, and MFB. (**D**) LBH (green) staining in cavernous tissues from two patients with diabetic erectile dysfunction and two patients with congenital penile curvature who had normal erectile function during reconstructive penile surgery. Scale bar, 100 µm. (**E**) LBH (red) staining in primary cultured human cavernous pericytes under NG and HG conditions for 3 days. (**F** and **G**) LBH immunopositive areas were quantified by Image J, and results are presented as means ± SEM (n = 4). Nuclei were labeled with DAPI (blue). The relative ratio in the control or NG group was defined as 1. ***$P < 0.001$. NG, normal glucose; HG, high glucose; DM, diabetes mellitus; DAPI, 4,6-diamidino-2-phenylindole.

Fig. 6. LBH-interacting protein identification in mouse cavernous pericytes. (**A**) LBH was immunoprecipitated (IP) from whole-MCPs lysates, resolved on SDS-PAGE gels, and stained with Coomassie blue solution. Gel bands indicated by red frame dot line were analyzed by liquid chromatography tandem mass spectrometry (LC-MS/MS) analysis. (**B**) IP of LBH from whole-MCPs lysates followed by immunoblot analysis to detect CRYAB and Vimentin. (**C** and **D**) Representative images of immunofluorescence staining of LBH (green)/CRYAB (red) and LBH (green)/VIM (red) in normal penis tissues and MCPs. Nuclei were labeled with DAPI (blue). Scale bar, 100 µm (top), 25 µm (bottom). (**E**) Protein-protein interaction network of LBH, CRYAB, VIM, and 1st and 2nd interactors of LBH. Lines connecting molecules show interaction sources in color. (**F**) Biological pathways involving molecules in PPI network identified by gene ontology analysis. (**G**) Significantly enriched gene sets associated with angiogenesis and nerve system in normal pericytes compared to diabetic pericytes in single cell data. (**H**) Representative western blots for CRYAB and VIM of MCPs under NG and HG conditions (left), and mouse penis tissues from age-matched control and diabetic mice (right). (**I**) Normalized band intensity ratio of CRYAB and VIM to β-actin was quantified using Image J, and results are presented as means ± SEM (n = 4). The relative ratio in the NG or control group was defined as 1. **$P < 0.01$; ***$P < 0.001$. MCPs, mouse cavernous pericytes; NG, normal glucose; HG, high glucose; DM, diabetes mellitus; DAPI, 4,6-diamidino-2-phenylindole.

Figure 1

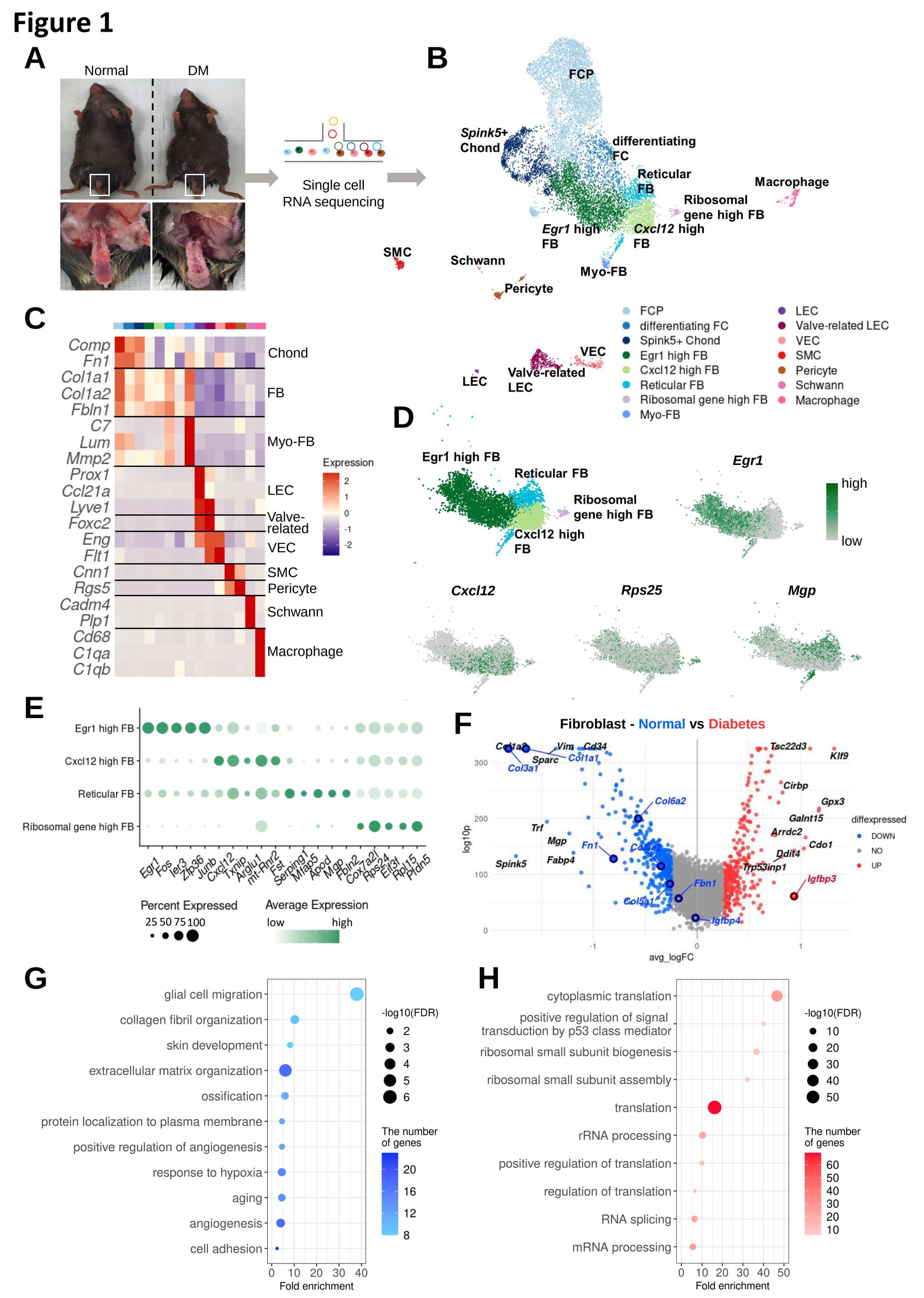
A
Normal
DM
Single cell
RNA sequencing
B
FCP
Spink5+
Chond
differentiating
FC
Reticular
FB
Macrophage
Ribosomal
gene high FB
Egr1 high
FB
Cxcl12 high
FB
SMC
Schwann
Myo-FB
Pericyte
VEC
LEC
Valve-related
LEC
FCP
differentiating FC
Spink5+ Chond
Egr1 high FB
Cxcl12 high FB
Reticular FB
Ribosomal gene high FB
Myo-FB
LEC
Valve-related LEC
VEC
SMC
Pericyte
Schwann
Macrophage
C
Comp
Fn1
Col1a1
Col1a2
Fbln1
C7
Lum
Mmp2
Prox1
Ccl21a
Lyve1
Foxc2
Eng
Flt1
Cnn1
Rgs5
Cadm4
Plp1
Cd68
C1qa
C1qb
Chond
FB
Myo-FB
LEC
Valve-related
VEC
SMC
Pericyte
Schwann
Macrophage
Expression
2
1
0
-1
-2
D
Egr1 high FB
Reticular FB
Ribosomal
gene high FB
Cxcl12 high
FB
Egr1
high
low
Cxcl12
Rps25
Mgp
E
Egr1 high FB
Cxcl12 high FB
Reticular FB
Ribosomal gene high FB
Egr1
Fos
Ier3
Zfp36
Junb
Cxcl12
Txnip
Arglu1
mt-Rnr2
Fst
Serping1
Mfap5
Apod
Mgp
Fbln2
Cox7a2l
Rps24
Eif3f
Rpl15
Pfdn5
Percent Expressed
25 50 75 100
Average Expression
low
high
F
Fibroblast - Normal vs Diabetes
Col1a2
Vim
Cd34
Sparc
Col1a1
Col3a1
Tsc22d3
Klf9
Cirbp
Gpx3
Galnt15
Arrdc2
Cdo1
Ddit4
Trp53inp1
Igfbp3
Col6a2
Trf
Mgp
Fn1
Col6a2
Spink5
Fabp4
Fbn1
Col5a1
Igfbp4
log10p
avg_logFC
diffexpressed
DOWN
NO
UP
G
glial cell migration
collagen fibril organization
skin development
extracellular matrix organization
ossification
protein localization to plasma membrane
positive regulation of angiogenesis
response to hypoxia
aging
angiogenesis
cell adhesion
Fold enrichment
-log10(FDR)
2
3
4
5
6
The number
of genes
20
16
12
8
H
cytoplasmic translation
positive regulation of signal
transduction by p53 class mediator
ribosomal small subunit biogenesis
ribosomal small subunit assembly
translation
rRNA processing
positive regulation of translation
regulation of translation
RNA splicing
mRNA processing
Fold enrichment
-log10(FDR)
10
20
30
40
50
The number
of genes
60
50
40
30
20
10

Figure 2

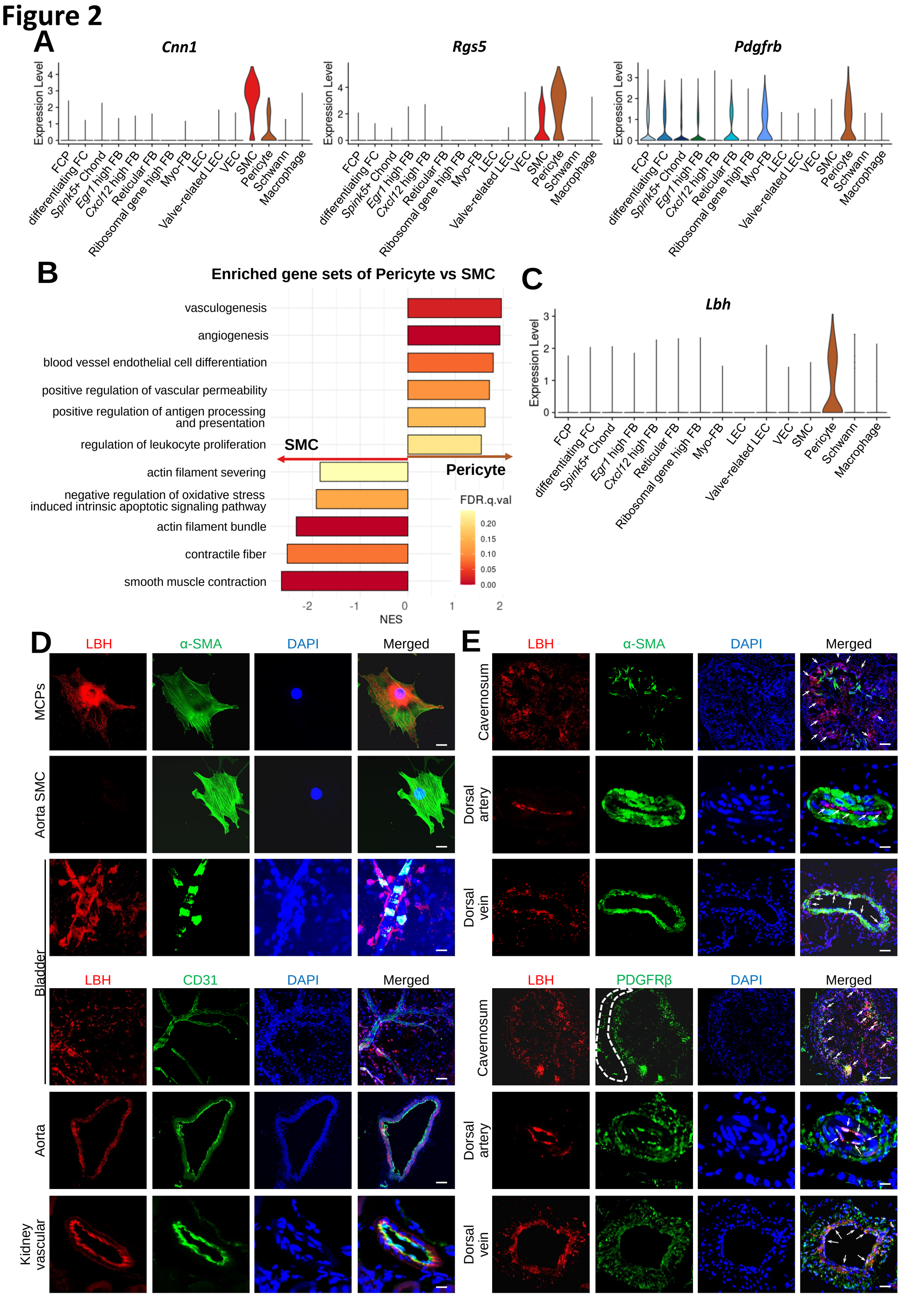
A
Cnn1
Rgs5
Pdgfrb
Expression Level
FCP
differentiating FC
Spink5+ Chond
Egr1 high FB
Cxcl12 high FB
Reticular FB
Ribosomal gene high FB
Myo-FB
LEC
Valve-related LEC
VEC
SMC
Pericyte
Schwann
Macrophage
B
Enriched gene sets of Pericyte vs SMC
vasculogenesis
angiogenesis
blood vessel endothelial cell differentiation
positive regulation of vascular permeability
positive regulation of antigen processing and presentation
regulation of leukocyte proliferation
actin filament severing
negative regulation of oxidative stress induced intrinsic apoptotic signaling pathway
actin filament bundle
contractile fiber
smooth muscle contraction
SMC
Pericyte
FDR.q.val
0.20
0.15
0.10
0.05
0.00
NES
C
Lbh
D
LBH
α-SMA
DAPI
Merged
MCPs
Aorta SMC
Bladder
CD31
Aorta
Kidney vascular
E
Cavernosum
Dorsal artery
Dorsal vein
PDGFRβ

Figure 3

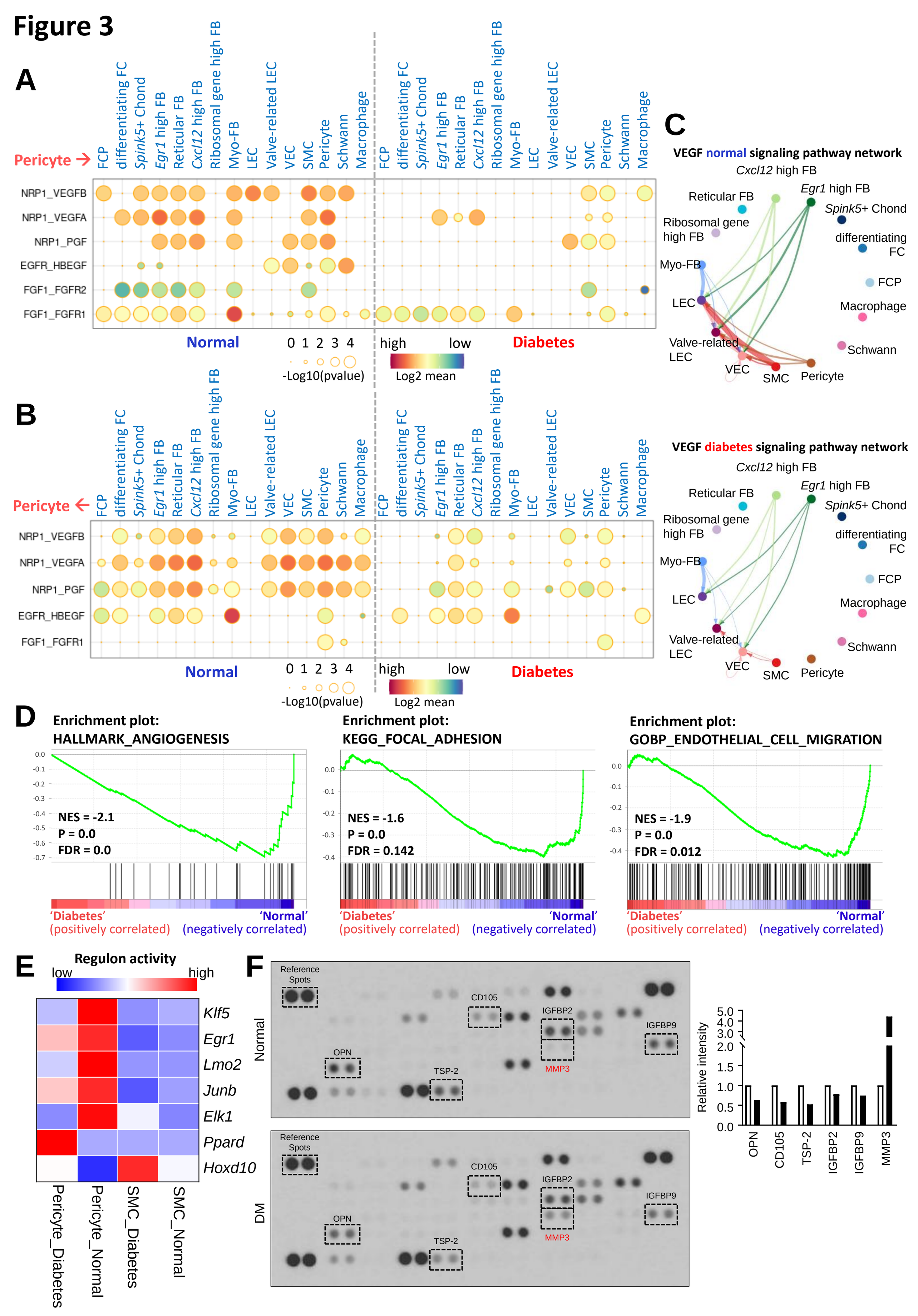
A
Pericyte →
FCP
differentiating FC
Spink5+ Chond
Egr1 high FB
Reticular FB
Cxcl12 high FB
Ribosomal gene high FB
Myo-FB
LEC
Valve-related LEC
VEC
SMC
Pericyte
Schwann
Macrophage
NRP1_VEGFB
NRP1_VEGFA
NRP1_PGF
EGFR_HBEGF
FGF1_FGFR2
FGF1_FGFR1
Normal
Diabetes
0 1 2 3 4
-Log10(pvalue)
high
low
Log2 mean
B
Pericyte ←
C
VEGF normal signaling pathway network
Cxcl12 high FB
Egr1 high FB
Reticular FB
Spink5+ Chond
Ribosomal gene high FB
differentiating FC
Myo-FB
FCP
LEC
Macrophage
Valve-related LEC
Schwann
VEC
SMC
Pericyte
VEGF diabetes signaling pathway network
D
Enrichment plot: HALLMARK_ANGIOGENESIS
NES = -2.1
P = 0.0
FDR = 0.0
Enrichment plot: KEGG_FOCAL_ADHESION
NES = -1.6
P = 0.0
FDR = 0.142
Enrichment plot: GOBP_ENDOTHELIAL_CELL_MIGRATION
NES = -1.9
P = 0.0
FDR = 0.012
'Diabetes' (positively correlated)
'Normal' (negatively correlated)
E
Regulon activity
low
high
Klf5
Egr1
Lmo2
Junb
Elk1
Ppard
Hoxd10
Pericyte_Diabetes
Pericyte_Normal
SMC_Diabetes
SMC_Normal
F
Reference Spots
CD105
IGFBP2
IGFBP9
OPN
TSP-2
MMP3
Normal
DM
Relative intensity
5.0
4.0
3.0
2.0
1.5
1.0
0.5
0.0
OPN
CD105
TSP-2
IGFBP2
IGFBP9
MMP3

Figure 4

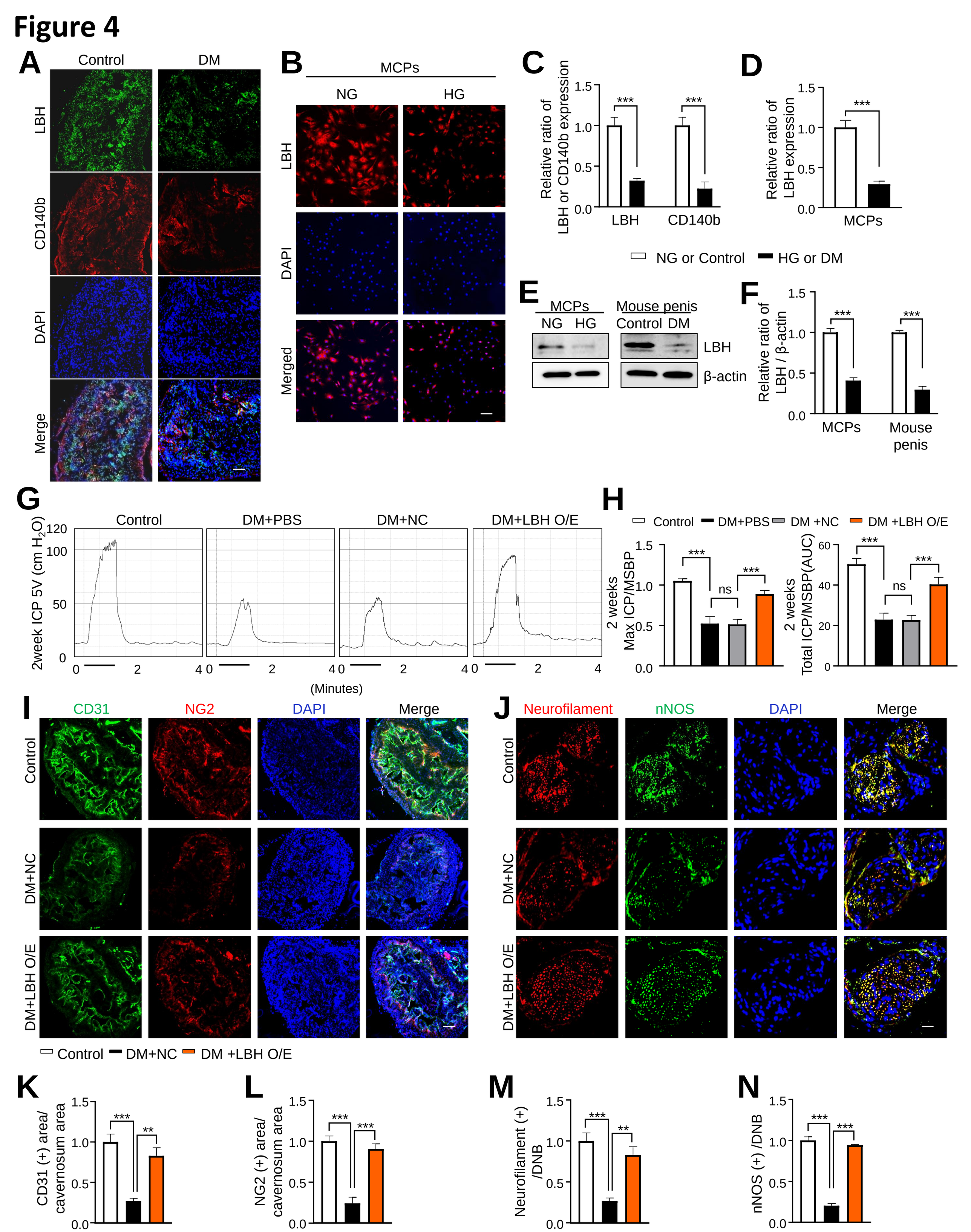
A
Control
DM
LBH
CD140b
DAPI
Merge
B
MCPs
NG
HG
LBH
DAPI
Merged
C
Relative ratio of LBH or CD140b expression
1.5
1.0
0.5
0.0
***
***
LBH
CD140b
D
Relative ratio of LBH expression
1.5
1.0
0.5
0.0
***
MCPs
NG or Control
HG or DM
E
MCPs
NG
HG
Mouse penis
Control
DM
LBH
β-actin
F
Relative ratio of LBH / β-actin
1.5
1.0
0.5
0.0
***
***
MCPs
Mouse penis
G
Control
DM+PBS
DM+NC
DM+LBH O/E
2week ICP 5V (cm H2O)
120
100
50
0
0
2
4
(Minutes)
H
Control
DM+PBS
DM +NC
DM +LBH O/E
2 weeks
Max ICP/MSBP
1.5
1.0
0.5
0.0
***
ns
***
2 weeks
Total ICP/MSBP(AUC)
60
40
20
0
***
ns
***
I
CD31
NG2
DAPI
Merge
Control
DM+NC
DM+LBH O/E
J
Neurofilament
nNOS
DAPI
Merge
Control
DM+NC
DM+LBH O/E
Control
DM+NC
DM +LBH O/E
K
CD31 (+) area/ cavernosum area
1.5
1.0
0.5
0.0
***
**
L
NG2 (+) area/ cavernosum area
1.5
1.0
0.5
0.0
***
***
M
Neurofilament (+) /DNB
1.5
1.0
0.5
0.0
***
**
N
nNOS (+) /DNB
1.5
1.0
0.5
0.0
***
***

Figure 5

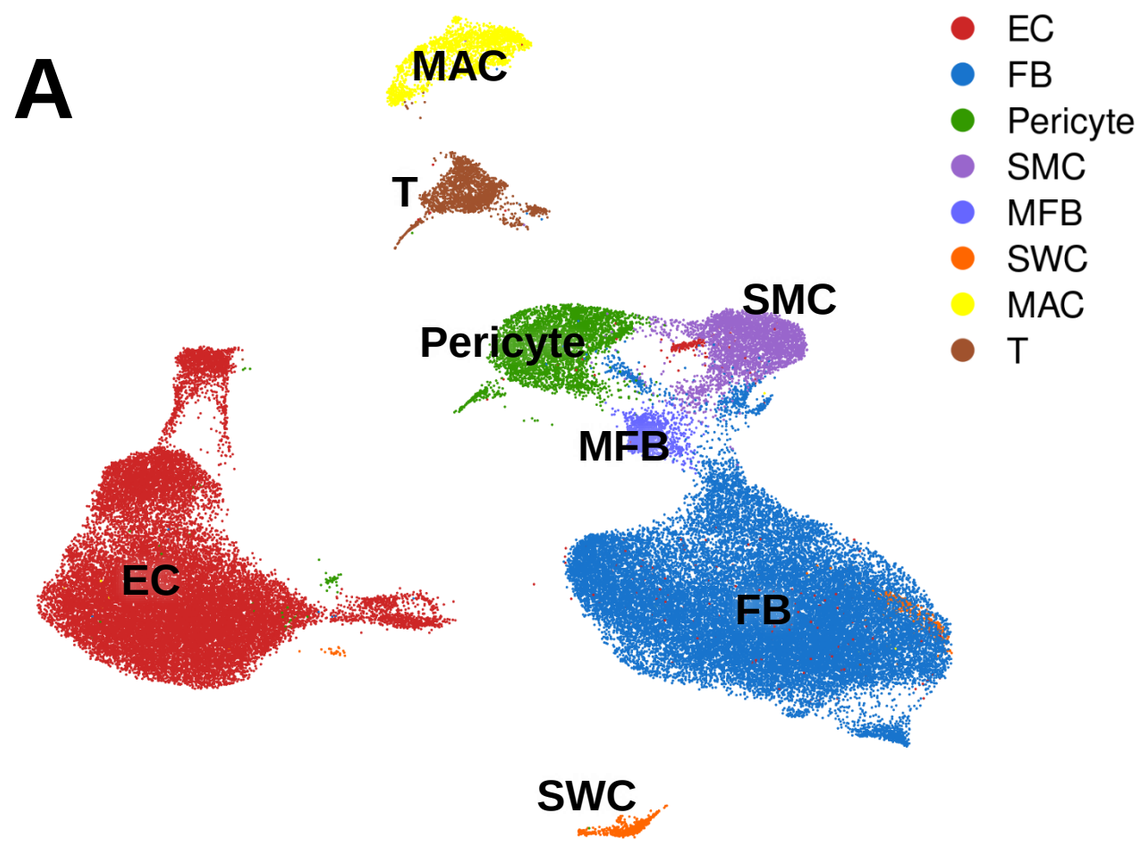

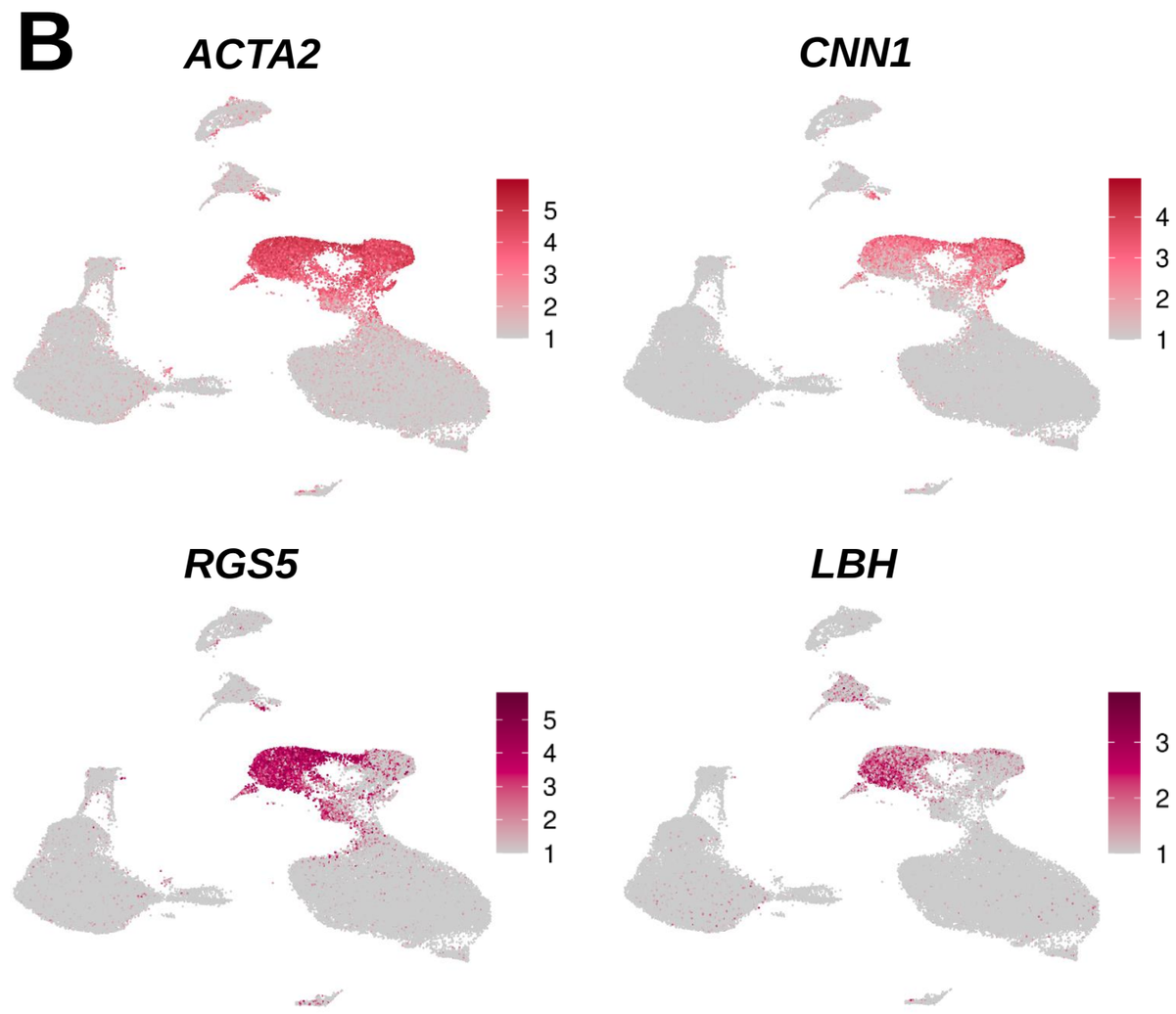

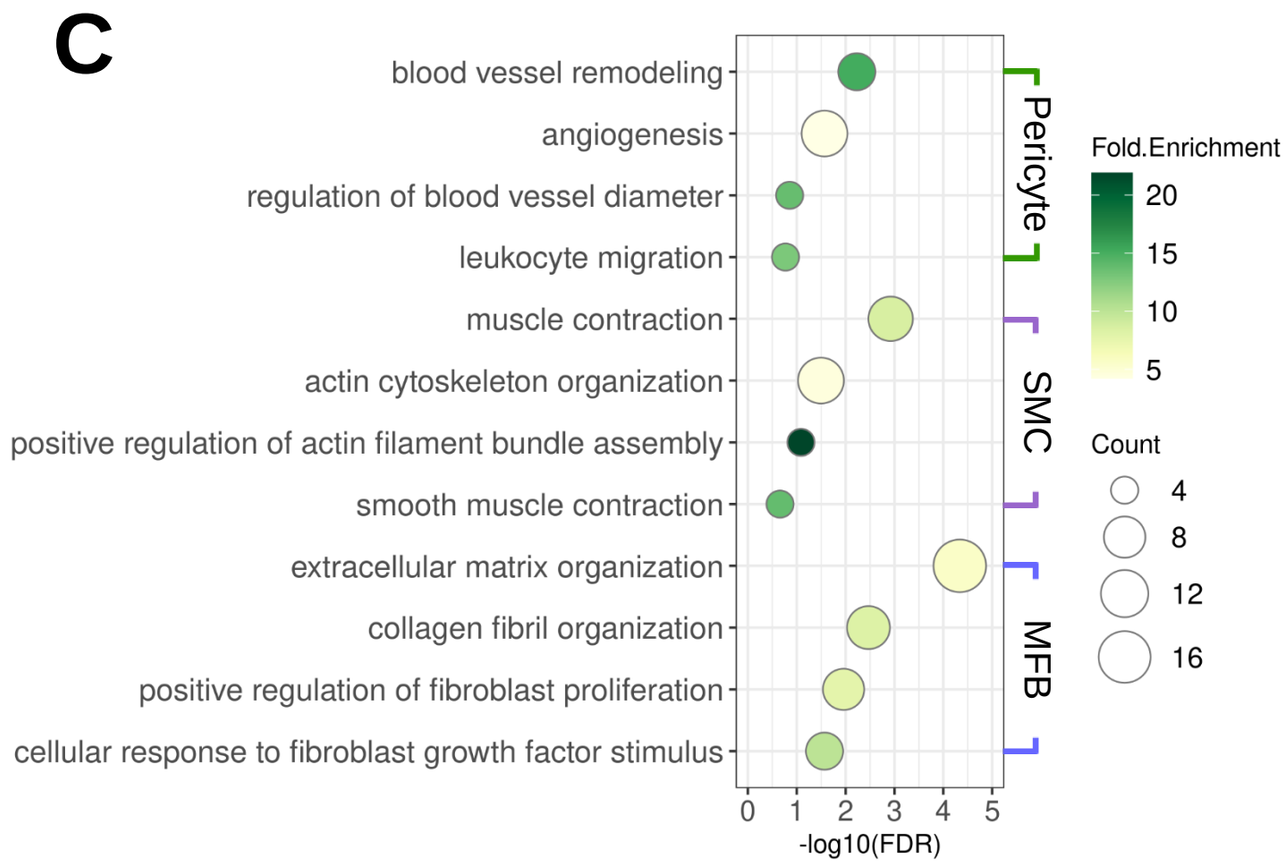

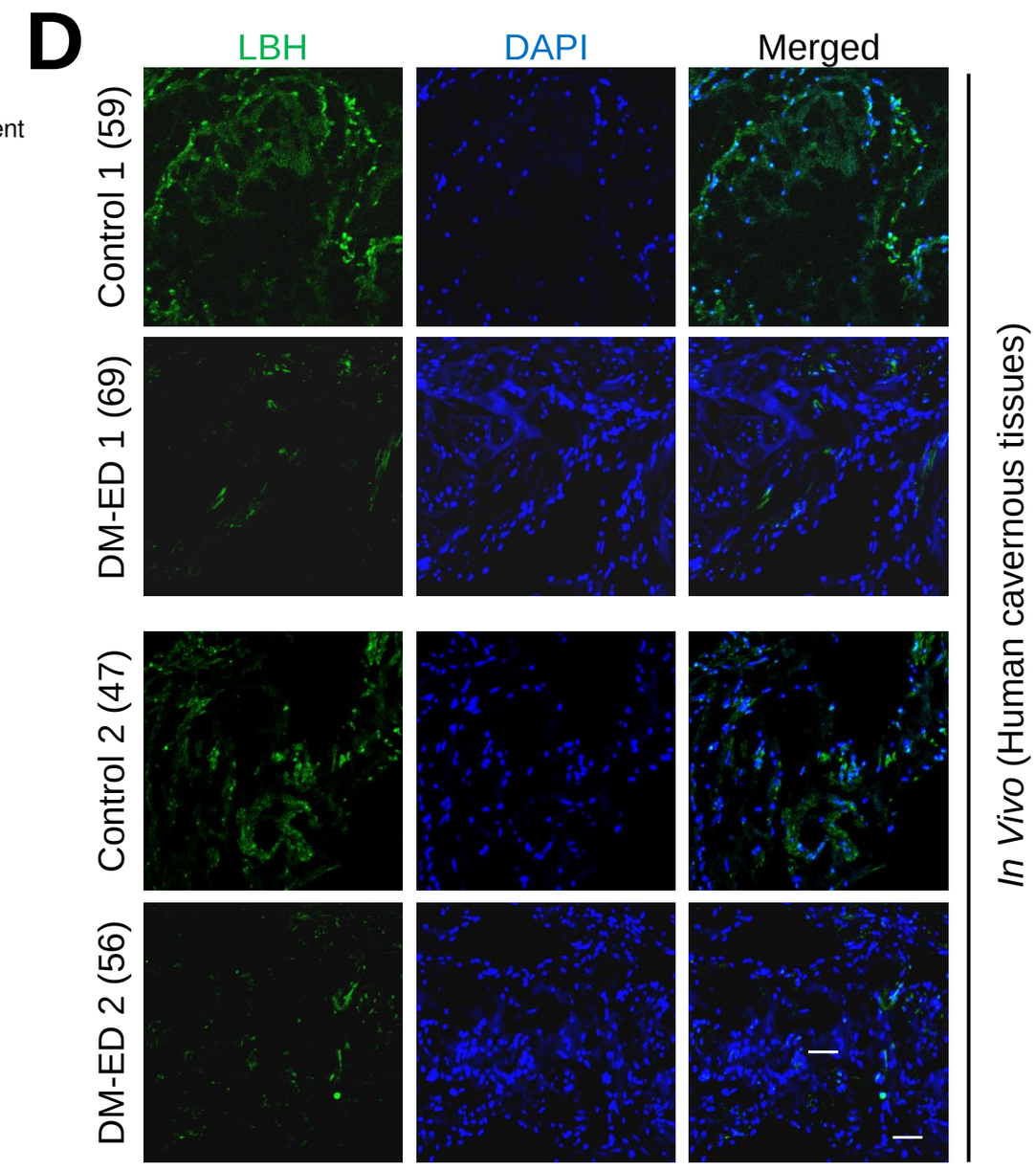

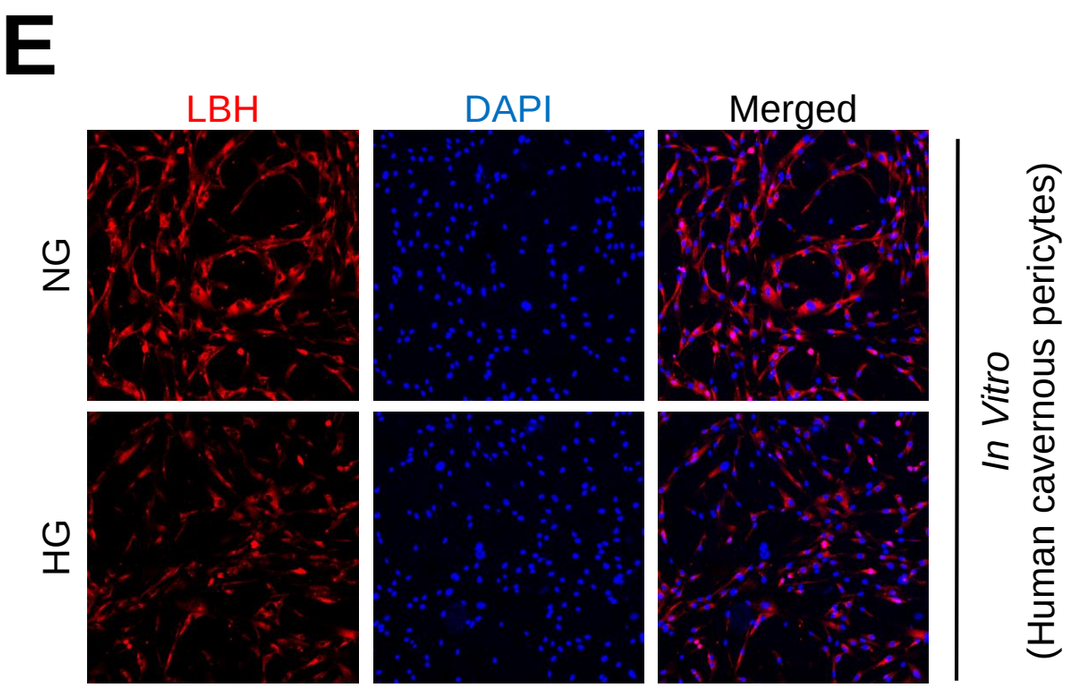

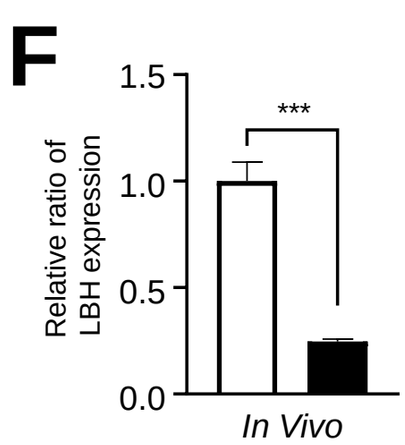

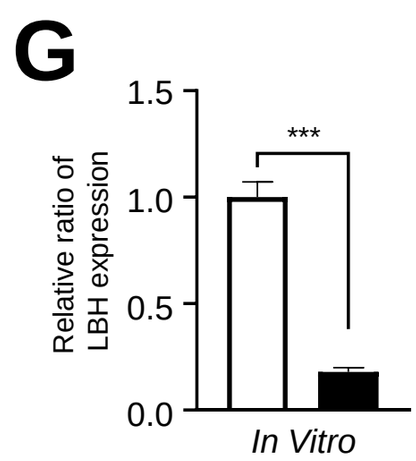

Control or NG DM-ED or HG

Figure 6

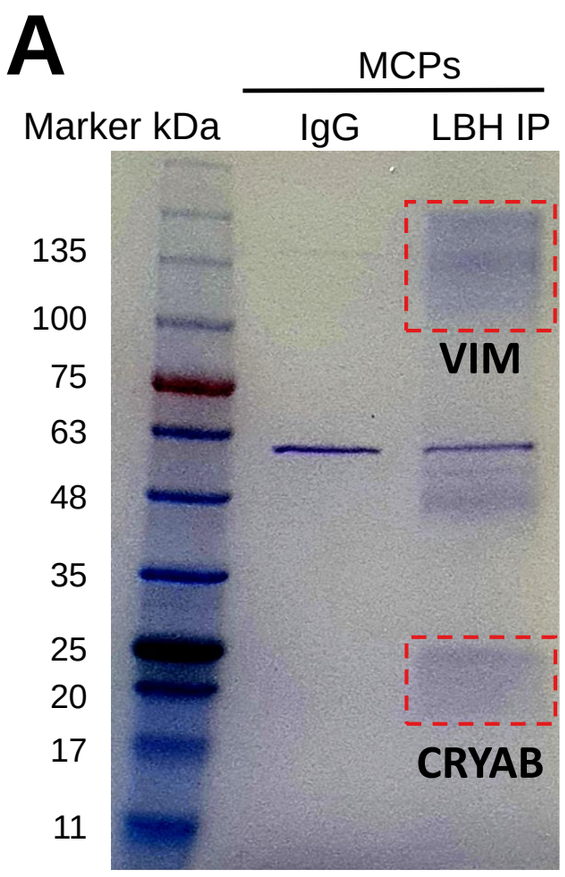
A
MCPs
Marker kDa
IgG
LBH IP
135
100
75
63
48
35
25
20
17
11
VIM
CRYAB

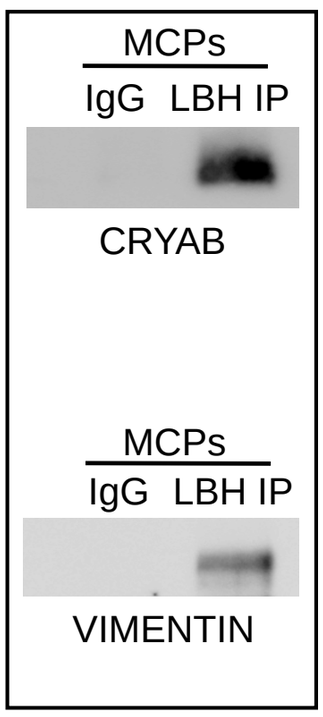
B
MCPs
IgG
LBH IP
CRYAB
MCPs
IgG
LBH IP
VIMENTIN

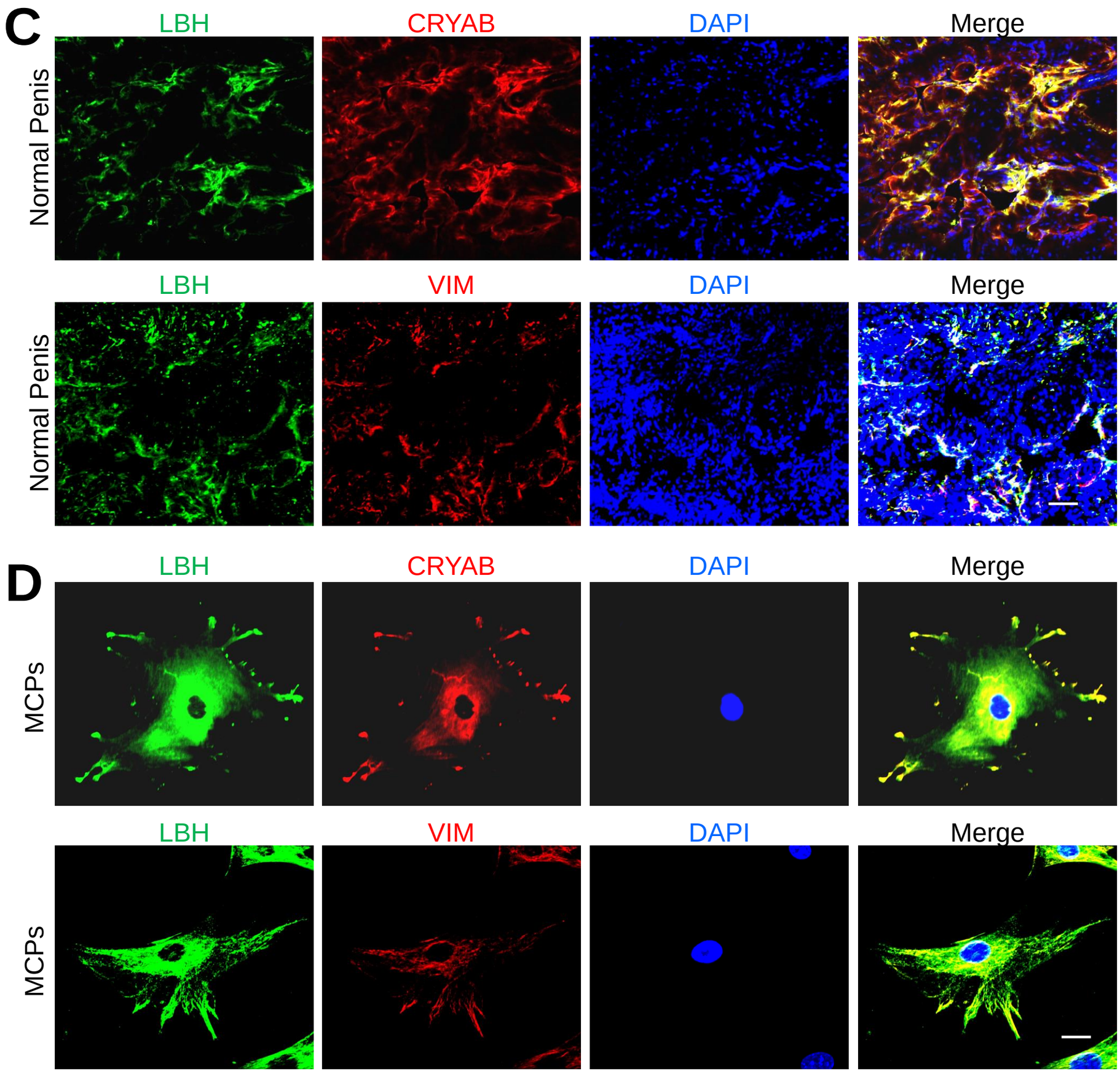
C
LBH
CRYAB
DAPI
Merge
Normal Penis
LBH
VIM
DAPI
Merge
Normal Penis
D
LBH
CRYAB
DAPI
Merge
MCPs
LBH
VIM
DAPI
Merge
MCPs

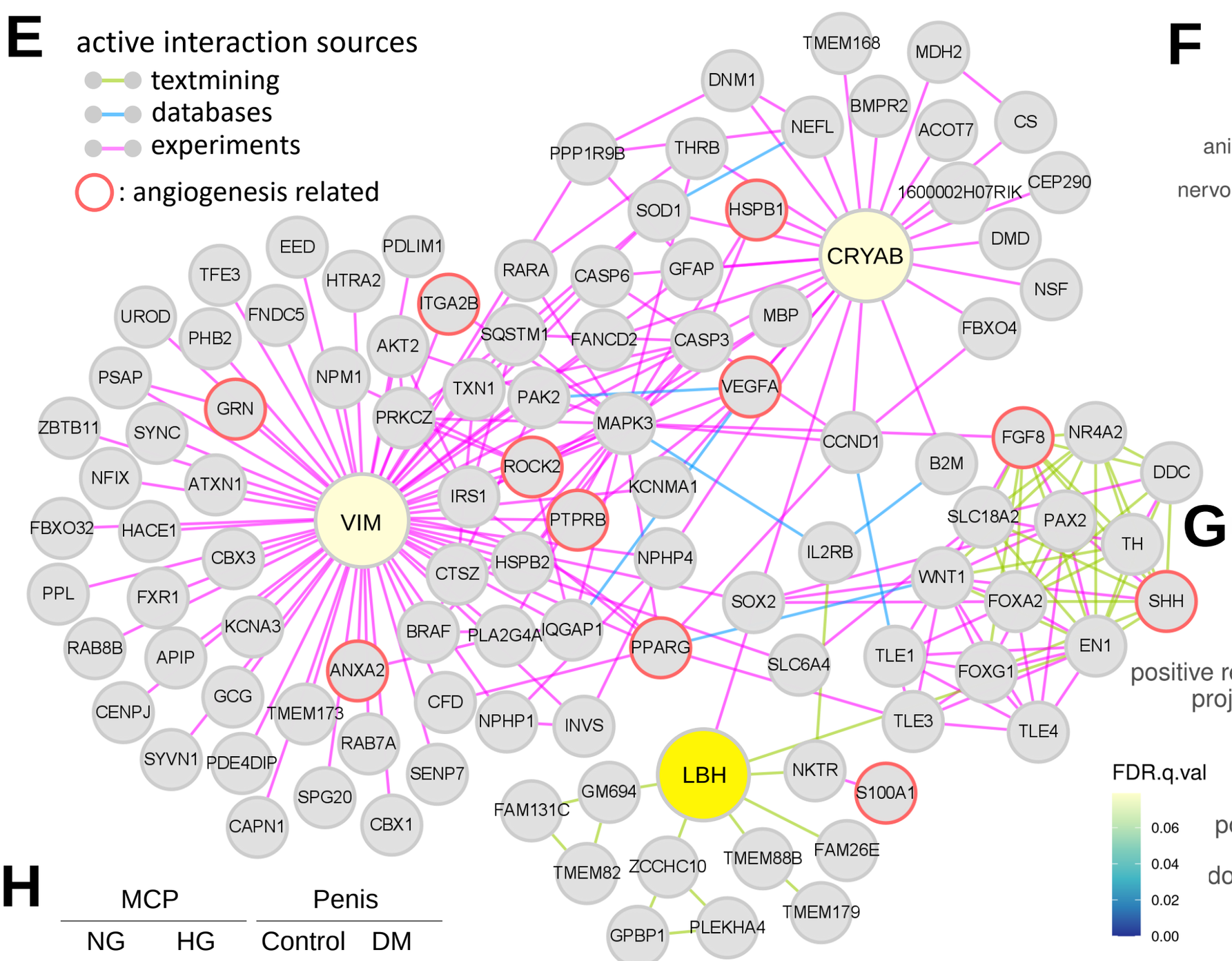
E
active interaction sources
textmining
databases
experiments
: angiogenesis related
CRYAB
VIM
LBH
TMEM168
MDH2
DNM1
BMPR2
NEFL
ACOT7
CS
PPP1R9B
THRB
CEP290
1600002H07RIK
SOD1
HSPB1
DMD
EED
PDLIM1
RARA
CASP6
GFAP
NSF
TFE3
HTRA2
ITGA2B
UROD
FNDC5
SQSTM1
FANCD2
CASP3
MBP
FBXO4
PHB2
AKT2
PSAP
NPM1
TXN1
PAK2
VEGFA
GRN
PRKCZ
MAPK3
ZBTB11
SYNC
CCND1
FGF8
NR4A2
B2M
DDC
NFIX
ATXN1
ROCK2
KCNMA1
IRS1
SLC18A2
PAX2
FBXO32
HACE1
PTPRB
TH
CBX3
NPHP4
IL2RB
HSPB2
CTSZ
WNT1
PPL
FXR1
SOX2
FOXA2
SHH
KCNA3
BRAF
PLA2G4A
IQGAP1
PPARG
EN1
RAB8B
APIP
SLC6A4
TLE1
FOXG1
ANXA2
GCG
CFD
TMEM173
NPHP1
INVS
TLE3
TLE4
CENPJ
RAB7A
SYVN1
PDE4DIP
SENP7
NKTR
S100A1
SPG20
GM694
FAM131C
CAPN1
CBX1
TMEM82
ZCCHC10
TMEM88B
FAM26E
TMEM179
GPBP1
PLEKHA4

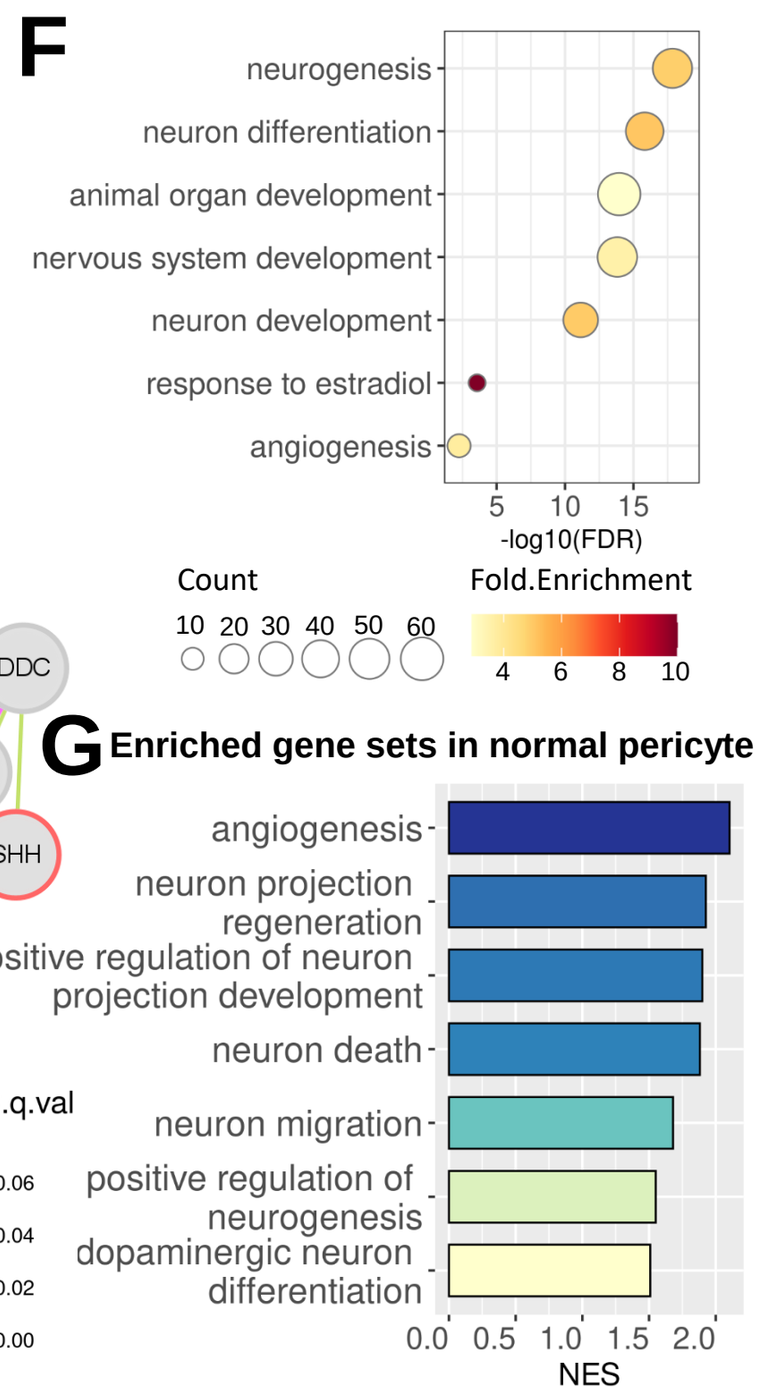
F
neurogenesis
neuron differentiation
animal organ development
nervous system development
neuron development
response to estradiol
angiogenesis
5
10
15
-log10(FDR)
Count
10 20 30 40 50 60
Fold.Enrichment
4 6 8 10
G
Enriched gene sets in normal pericyte
angiogenesis
neuron projection regeneration
positive regulation of neuron projection development
neuron death
neuron migration
positive regulation of neurogenesis
dopaminergic neuron differentiation
0.0 0.5 1.0 1.5 2.0
NES
FDR.q.val
0.06
0.04
0.02
0.00

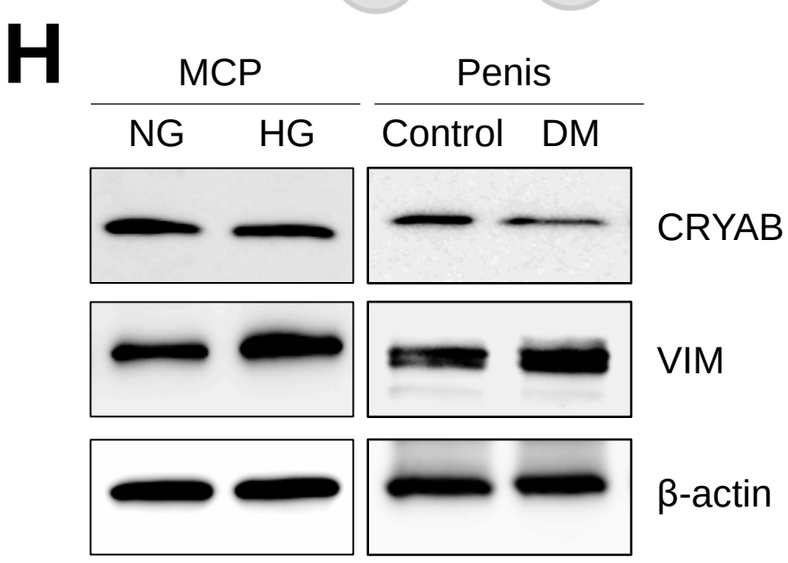
H
MCP
Penis
NG
HG
Control
DM
CRYAB
VIM
β-actin

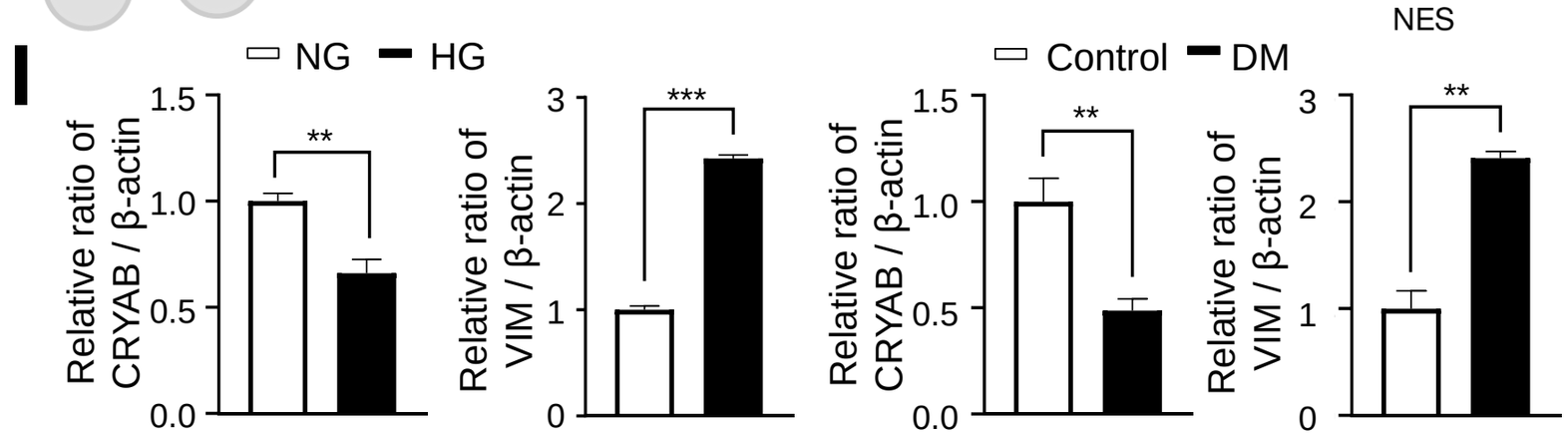
I
NG
HG
Relative ratio of CRYAB / β-actin
1.5
1.0
0.5
0.0
**
Relative ratio of VIM / β-actin
3
2
1
0
***
Control
DM
Relative ratio of CRYAB / β-actin
1.5
1.0
0.5
0.0
**
Relative ratio of VIM / β-actin
3
2
1
0
**